Russian Chemical Reviews **82** (6) 483 – 510 (2013) © 2013 Russian Academy of Sciences and Turpion Ltd

DOI 10.1070/RC2013v082n06ABEH004351

Phonons on the clean metal surfaces and in adsorption structures

G G Rusina, E V Chulkov

Contents

I.	Introduction	483
II.	Brief historical account	484
III.	Theoretical methods for the calculation of surface phonons	486
IV.	Results of investigations of surface phonons	489
V.	Conclusion	506

Abstract. The state-of-the-art studies of the vibrational dynamics of clean metal surfaces and metal surface structures formed upon the sub-monolayer adsorption of the atoms of various elements are considered. A brief historical survey of the milestones of investigations of surface phonons is presented. The results of studies of the atomic structure and vibration characteristics of surfaces with low and high Miller indices and adsorption structures are analyzed. It is demonstrated that vicinal surfaces of FCC metals tend to exhibit specific vibrational modes located on the step and polarized along the step. Irrespective of the type and position of adsorption or the substrate structure, the phonon spectra of sub-monolayer adsorption structures always tend to display two modes for combined translational displacements of adatoms and for coupled vibrations of substrate atoms and adatoms polarized in the direction normal to the surface. The bibliography includes 202 references.

I. Introduction

Surface or crystal/vacuum interface dynamics is a very important area of solid state physics and chemistry. When a surface is formed, the number of nearest neighbours of external layer atoms decreases. This breaks the symmetry of distribution of masses and forces that act on a surface atom from the other atoms. In addition, interatomic interactions on a free surface change upon its structural relaxation and/or reconstruction. A change in the type and number of interatomic bonds may alter the coordination number of surface atoms, especially in the presence of defects such as steps and adatoms. The listed factors result in crucial differences between the dynamic properties on the surface and in the bulk; in particular, the energy of the normal vibrational modes of the crystal lattice near the surface markedly decreases and a new class of vibrational modes appears, which were called surface phonons.

The surface phonons are vibrational excitations in which the amplitude of atomic displacements is maximum on the surface but exponentially decreases in the bulk.[1,2] Study of the surface phonon spectrum provides information about the atomic structure, type of bonds and force constants in the surface layers. These characteristics determine the structure and phase transformations on the surface and the surface resistance to external effects. Detailed knowledge of the dynamic properties of the surface is needed in all cases where the surface plays an important role — for the design of electronic and optical instruments, for heterogeneous catalysis, photochemical reactions, charge and spin transfer processes over the surfaces and through interfaces and for materials science.

Vigorous research of the vibrational properties of the surface was started at the end of the 20th century and still goes on. There are objective reasons responsible for the persistent attention to the surface phonons. The advent of new experimental methods and increase in the resolving power of existing methods such as low-energy electron diffraction, inelastic helium atom scattering, high resolution electron energy loss spectroscopy, photoelectron spectroscopy, inelastic tunnelling spectroscopy/microscopy provide the possibility of more accurate measurements of the surface atomic structure and dispersion curves for increasing number of materials. The increase in the accuracy of theoretical methods, which permit direct comparison of theoretical and experimental data, stimulates investigation of surface phonon-related phenomena. With the advent of supercomputers, it became possible to carry out calcula-

G G Rusina Institute of Strength Physics and Materials Science, Siberian Branch of the Russian Academy of Sciences, Akademichesky prosp. 4/2, 634021 Tomsk, Russian Federation; Tomsk State University, prosp. Lenina 36, 634050 Tomsk, Russian Federation. Tel. (7-3822) 28 69 43, e-mail: rusina@ispms.tsc.ru
E V Chulkov Donostia International Physics Center (DIPC) 20018 San Sebastián/Donostia, Paseo de Manuel Lardizabal 4, Spain
Faculty of Chemistry of the University of the Basque Country, 20080 San Sebastián/Donostia, Apartado 1072, Spain.
Tel. (7-34934) 01 82 20, e-mail: waptctce@eh.es

Received 3 October 2012
Uspekhi Khimii **82** (6) 483 – 510 (2013); translated by Z P Svitanko

tions for the surface force constants and phonon dispersion curves not only for atomically smooth but also for defective surfaces — having steps, kinks and adsorbates.

Methods based on density functional theory (DFT), in particular, methods of *ab initio* molecular dynamics, self-consistent linear response and frozen phonons have been applied most extensively to surface phonon investigations. Apart from *ab initio* methods, model approximations using both parametric data and density functional theory are being actively developed.

Quite a lot of information about equilibrium structures and dynamics of clean metal surfaces has been accumulated to date. Data on the structures and vibrational properties of metal surfaces with adsorbates are much more scarce. Lately, surfaces of exactly this type have received considerable attention of theorists and experimentalists. The reviews [3–5] on surface phonons published before 2003 describe the experimental and theoretical methods for determination of dispersion curves for both clean metal and semiconductor surfaces and adsorbate-bearting surfaces and also present the dispersion curves for some materials. More recently, new data appeared, which markedly supplemented the views on surface phonons.

The purpose of this work is to acquaint the interested readers with the latest achievements in investigations of the surface dynamics and, on the basis of analysis of published data, to draw general conclusions, which could be useful for better understanding of the mechanisms of surface phenomena and processes. The dependence of surface dynamics on the chemical nature of the material, crystallographic orientation of faces and the presence of steps and adatoms on the surface is discussed in detail. In terms of a unified approach (which avoids ambiguous data interpretation), modifications of the vibrational characteristics of the surface upon complication of the surface structure and in the presence of adsorbed structures are analyzed. An earlier review [4] surveyed in considerable detail the relaxation and dynamics of simple (low Miller index) metal surfaces; therefore, in the present review, this issue is addressed to an extent that is necessary for the understanding of the ground principles of formation of the phonon structure and its dependence on the crystallographic orientation of the surface and the chemical type of the metal. Primary attention is paid to phonons in vicinal (high Miller index) surfaces and in superstructures that are formed upon sub-monolayer adsorption of one metal onto another.

The review is composed in the following way. Section II gives a brief historical account of the milestones of experimental and theoretical studies of phonons on metal surfaces. We believe that this review covering not only the last 10–15 years but also much earlier years will be useful for comprehensive perception of the evolution of this important area of metal surface physics and chemistry. Section III deals with the key aspects of the microscopic theory of surface phonons and various approaches for their theoretical description. One of the semiempirical methods used widely and successfully for the construction of interatomic interaction potentials that are needed for calculating the structural relaxation and surface phonons, the so-called embedded atom method, is described in detail. Section IV gives the results of calculations of the structural relaxation and phonon spectra for simple and vicinal surfaces for some FCC metals and for the surface structures formed by alkali metal adatoms on low Miller index surfaces. The obtained results are compared with the results of experiments and *ab initio* calculations (continuous testing of the adequacy of model potentials is performed in this way). The generalizing conclusions about the phonon structures of metal surfaces and modification of their vibrational properties on going from chemically pure and smooth metal surfaces to surfaces having steps and adsorbates are presented in the Conclusion, which also discusses the prospects of the development of the theory of surface phonons as applied to electron–phonon interactions and metal cluster dynamics.

II. Brief historical account

The dynamic processes on the surface have long aroused the interest of natural scientists. Rayleigh,[6] who studied the propagation of acoustic waves along the surface of an elastic isotropic medium in 1887, was one of the first to consider these processes. In the long-wave limit, the solution of the equation of motion gives a vibrational mode corresponding to displacements in the sagittal plane (the plane containing the Rayleigh wave vector and the normal to the surface). In 1911, Love [7] studied the type of surface waves (Love waves) that arise when a macroscopic layer of a material is deposited on the surface of another material. Finally, in 1924 Stoneley [8] considered the type of waves (Stoneley waves) that propagate along the interface between two materials. Only a quarter of a century later, was surface dynamics further developed in the works of Livshitz and Rozentsveig,[1] Maradudin *et al.*,[2] and Wallis,[9] who theoretically substantiated the existence of localized surface phonon states. In 1971, Allen and co-workers [10–12] proposed a classification of surface vibrational modes in which they distinguished true surface states (the maximum localization of the vibrations on the surface and fast decay in the bulk) and surface resonances (predominant surface localization and deep penetration into the bulk).

With the advent in the 1980s of experimental methods able to detect vibrations of surface atoms and to determine the dynamic characteristics of these atoms, vigorous research of the surface dynamics started. These methods are based on measurement of the inelastic component of scattering of low-energy particles (atoms, molecules, electrons) by surface atoms. The distribution of scattered particles (*e.g.*, electrons) would be different depending on whether they are scattered by short-wave vibrations of lattice atoms that create space-localized potential fluctuations or by long-wave vibrations of surface charges.

Among the multitude of experimental methods for the study of surface dynamics, the most widely used are inelastic He atom scattering (HAS) [13–15] and electron energy loss spectroscopy (EELS).[16] The HAS technique is used to study the surface phonons in metals, ionic crystals and semiconductors.[13–15,17–20] The EELS method was first employed in 1971 to study the phonons of a reconstructed Si(111) surface [21] and later for determining the dispersion curves (phonon spectra) for clean metal surfaces [22,23] and for the surfaces bearing adatoms and molecules.[24–27] In the last decade, inelastic electron tunnelling spectroscopy (IETS) [28] and inelastic electron tunnelling spectroscopy–scanning tunneling microscopy (IETS-STM) proposed in 1986 by Hamers *et al.*[29] have been actively used. These methods are utilized most beneficially to determine the vibrational characteristics of adsorbates.[30]

Theoretical investigations of surface phonons develop in parallel with experimental studies, because, on the one hand, they serve as the basis for interpretation of the obtained results and, on the other hand, they stimulate new experiments. In the general form, the theory of surface dynamics of crystals includes several levels that differ by the number of parameters determined beyond the theory, *e.g.*, in experiment. One end of this raw is occupied by the phenomenological method of Born–von Karman force constants,[31] while the other end belongs to *ab initio* calculations of phonon spectra and other lattice characteristics.[4] Between these extremes are the semiempirical model theories in which the description of interatomic interactions in the condensed medium is based on the idea of the dependence of the system energy on the electron density.[32–34] The force constant method was first used by Maradudin *et al.*[2] and Wallis[35] for the studies of low Miller index surfaces of FCC metals.

A great contribution to the surface phonon theory was made by Black and Wallis,[36–38] who employed various force constant models; the most complex model took into account the interactions up to the third coordination sphere. The calculations for (100), (110) and (111) surfaces for a number of BCC and FCC structures were carried out, parameters of the method being adjusted to experimental data as regards elastic characteristics and phonon modes of the bulk material. As was shown,[13–15,20–23] the results obtained by the force constant method are qualitatively in rather good agreement with the experimental data for these surfaces. However, while being rather simple, this method does not take into account the changes in the force constants on the surface and charge density redistribution caused by the bond rupture. The relationship between the change in the calculated values of electron density and the change in force constants is taken into account by itself in the *ab initio* self-consistent methods;[4,39] however, their applicability is mainly restricted to simple surfaces, as more complex surface structures require an extended unit cell basis and bring about the necessity to take into account a large number of atoms, which requires too much computation time.

In model calculation methods such as the effective medium theories (EMT)[32] and embedded atom method (EAM),[33] the tight-binding approximation (TBA),[34] the total energy of a system is determined by the sum of pair potentials and the atomic energy. The atomic energy depends on the local electron density of the atom embedded into the electron density created by all other atoms. This approach describes the many-particle character of interatomic interactions and takes account of the electronic contribution to the structural relaxation of the surface. The model methods are plain, provide high computation rate and correctly reproduce the key atomic characteristics of the bulk metal: elastic constants, the equilibrium lattice parameters, bond energy and the vacancy formation energy. The key shortcoming of these methods, namely, the non-self-consistent construction of the electron density, preclude the accurate description of redistribution of charge density or change in the shielding properties.[33] However, these methods use characteristics (lattice parameters, elastic constants, vacancy formation energies) that are adjusted to experimental data and, hence, self-consistency may be effectively taken into account in the construction of charge density.

The studies of metal surface phonons that are considered in this review successfully use the EAM[33] and its modifications.[40] The calculations of the vibrational states on low Miller index surfaces[41–45] demonstrated that the EAM affords for such surfaces a phonon structure that is in good agreement with experimental[15–23] and *ab initio* calculation results.[4,39] Even more effective is the application of EAM to calculate the vibrational states of the high Miller index surfaces,[46,47] surface structures, interfaces and adsorbed clusters.[48–57]

The first theoretical investigations of the phonon structure of vicinal surfaces were performed by Black and Bopp[58] and Knipp.[59] They used the force constant method to calculate the phonon spectra of perfect vicinal surfaces of a model FCC crystal and introduced the notion of step mode, which is a mode that propagates along steps and does not penetrate to the terrace. Most of the theoretical data on the vicinal surface dynamics were obtained using semiempirical models[5,47,60] and *ab initio* calculations.[61,62]

While exploring various aspects of sub-monolayer adsorption, systems containing alkali metal atoms (Li, Na, K, Cs) adsorbed on a metal surface are often considered as models.[63–71] The interest in these systems is not accidental, because they represent the simplest type of chemical adsorption. At low coverages (θ) by the alkali metal ($\theta \leqslant 1$ monolayer), lattices with large periods in which the adatoms occupy identical adsorption sites are formed, which is suitable for investigating the nature of adsorbate–substrate interactions.[72] The adsorption of alkali metals induces electron density redistribution on the surface and, as a consequence, the physical properties of the surface change crucially and various quantum effects are manifested. It was shown[73–76] that adsorption of sodium on the Al(100) and Cu(111) surfaces results in the formation of quasi-two-dimensional electronic states with long lifetimes. The alkali metal adatoms affect the electron–electron and electron–phonon interactions, the mechanism of electron/hole excitation being often changed.[77–80] Alkali metals also play a significant role in heterogeneous catalysis:[81] they substantially accelerate catalytic reactions on metal surfaces and decrease the electron work function of the substrate surface.

Data on more than 60 geometries of alkali metal adsorption on metal surfaces are available to date; analysis of these data is useful for better understanding of the bonding of alkali metals to the metallic substrate. However, it is still difficult to exactly predict the type of adsorption structure: depending on the position of adsorption, it can be formed according to substitutional pattern (to give a surface alloy) or adatom adsorption pattern (to give a surface structure).[70,82–84] Apart from the data on atomic structure, experimental and theoretical information on the electronic structure of such systems has been gained.[83,84] Their dynamics has been studied to a much lesser extent (due to the complexity of experimental and theoretical procedures).

Toennies and co-workers[63–65] performed a series of experimental works devoted to the dynamics of adsorbed alkali metal films ($\theta = 2–20$ monolayers). Using the HAS method, growth conditions of sodium, potassium, rubidium and caesium thin films on the Cu(100) surface were studied. An unusual vibrational mode was found in the film ($\theta > 5$ monolayers) and interpreted as collective motion of atoms. The behaviour of this mode resembles the behaviour of the Einstein oscillator, its frequency being independent of the

total parallel momentum transferred to the substrate surface. The authors defined this mode as a longitudinal acoustic standing wave arising upon simultaneous synphasic displacements of the film atoms (longitudinal) and the substrate atoms (vertical) and propagating normally to the film surface. The mode and overtone frequencies were directly dependent on the film thickness and reflected information about the force constants in the film and at the interface with the substrate. A specific feature of the identified mode is the transverse displacement of adatoms caused by the energy transfer from the high-frequency stretching S-mode to the translational T-mode. As a result of this interaction, it was classified as the frustrated translational mode (FT mode). It is this mode that determines the possibility of adatom migration over the substrate surface.

Some authors [66–68] used the HAS method to study the phonon dispersion upon the adsorption of sodium, potassium and caesium monolayers on Ni(111) and Cu(111) surfaces. In this case, the frustrated translational mode, similar to the mode of multilayer films, was also determined. Not less interesting results were obtained for submonolayer degrees of adsorption ($\theta \leqslant 1$ monolayer) where ordered adsorption structures are formed. The most comprehensive experimental studies were carried out for aluminium surfaces with lithium, sodium and potassium adatoms. Using transitional methods such as low-energy electron diffraction (LEED), scanning tunnelling microscopy (STM) and EELS, for these structures only the high-frequency S-mode polarized strictly perpendicularly to the surface and corresponding to hybridized displacements of the adatom and nearest substrate atoms was identified.[69] This result was not unexpected, because the sensitivity of the methods used is suitable for the clear-cut interpretation of only high-energy vertical vibrational modes. The excitation energy of the FT mode was shown [63–65] to depend on the film thickness and may be expected to be very low in the case of sub-monolayer adsorption. However, Nagao *et al.* [85] were able to measure the energy of the FT mode for the ordered structures formed upon sub-monolayer adsorption ($\theta = 1/3 - 1/2$ monolayers) of sodium and lithium on the Al(111) surface using high resolution electron energy loss spectroscopy (HREELS). Finberg *et al.*[69] used the HAS method to determine the energy of the translational mode for potassium adsorption ($\theta = 1/3$ monolayers) on the Al(111) surface. The energy of the FT mode actually proved to be low, being $\sim$3.1 and $\sim$2.3 meV for sodium and potassium adsorption, respectively.

The experimental determination of the equilibrium bond lengths of the adsorbate and the substrate and the energies of some vibrational modes, which can serve for testing the calculation methods, stimulated further theoretical investigations of dynamic characteristics of adsorption structures. The first attempts of theoretical analysis of the adsorbate dynamics made use of simple force constant models considering the interaction of the first neighbours.[86, 87] Nagao *et al.*[85] performed calculations for sodium adatoms on the Al(111) surface with a periodicity of $(\sqrt{3}\times\sqrt{3})$R30° in parallel with HREELS experiment. However, these calculations described the localized vibrational states only at the centre of the Brillouin zone (BZ), and this precluded estimation of the dynamic stability of the adsorption structure along all directions. The *ab initio* calculations [3, 4] are also mainly limited to the BZ zone centre (point $\bar{\Gamma}$) due to the necessity to take into account a large number of atoms in the unit cell. Owing to their simplicity and efficiency, semiempirical methods dominate in the studies of vibrational structure of adsorbate-bearing surfaces.[53–56] Unlike *ab initio* approaches, they are suitable for calculation (requiring acceptable computation and time resources) of the dispersion curves along all of the symmetrical directions of the two-dimensional Brillouin zone for the unit cells with a large basis.

III. Theoretical methods for the calculation of surface phonons

1. Principal aspects of the microscopic theory of lattice dynamics

The microscopic theory of lattice dynamics is based on two approximations — adiabatic and harmonic ones. The calculation of crystal energy in the adiabatic approximation (Born–Oppenheimer)[88] is based on the idea of adiabatic separation of slow motion of ions and fast motion of valence electrons. In this case, the motion of atoms in the system is determined by the effective potential $V_{\text{ef}}\{\mathbf{R}\}$, which depends only on the ion coordinates $\{\mathbf{R}\}$. In the harmonic approximation, the effective potential describes the spectrum of phonon excitations of the crystal. Expansion of this potential into the Taylor series is restricted to the quadratic term for small atomic displacements $\mathbf{S}_{m\alpha}$ from the equilibrium position $\mathbf{R}^0_m$:

$$V_{\text{ef}}(\{\mathbf{R}\}) = V_{\text{ef}}(\{\mathbf{R}^0\}) + \sum_{m\alpha i} \frac{\mathrm{d}V}{\mathrm{d}R_{m\alpha i}}\bigg|_{\mathbf{R}_{m\alpha}=\mathbf{R}^0_{m\alpha}} S_{m\alpha i} + \\ + \frac{1}{2}\sum_{m\alpha i,\, n\beta j} \frac{\mathrm{d}^2V}{\mathrm{d}R_{m\alpha i}\mathrm{d}R_{n\beta j}}\bigg|_{\mathbf{R}_{m\alpha}=\mathbf{R}^0_{m\alpha},\, \mathbf{R}_{n\beta}=\mathbf{R}^0_{n\beta}} S_{m\alpha i}\cdot S_{n\beta j} + \ldots \qquad (1)$$

Here $\mathbf{R}_{m\alpha}$ is the position of atom α in unit cell m

$$\mathbf{R}_{m\alpha} = \mathbf{R}^0_{m\alpha} + \mathbf{S}_{m\alpha}$$

$$\mathbf{R}^0_{m\alpha} = \mathbf{R}^0_m + \boldsymbol{\tau}^0_\alpha$$

The subscript 0 implies the equilibrium position of unit cell m; the position of atom α in unit cell m is specified by the vector $\boldsymbol{\tau}^0_\alpha$, while the atomic displacement is determined by the vector $\mathbf{S}_{m\alpha}$. The values $R_{m\alpha i}$, $R^0_{m\alpha i}$, $S_{m\alpha i}$ are components of the vectors $\mathbf{R}_{m\alpha}$, $\mathbf{R}^0_{m\alpha}$, $\mathbf{S}_{m\alpha}$, respectively. The dynamic properties are determined by the force constants

$$\Phi^{\mathbf{h}}_{\alpha i,\,\beta j} = \frac{\mathrm{d}2V}{\mathrm{d}R_{m\alpha i}\mathrm{d}R_{n\beta j}}\bigg|_{\mathbf{R}_{m\alpha}=\mathbf{R}^0_{m\alpha},\, \mathbf{R}_{n\beta}=\mathbf{R}^0_{n\beta}} \qquad (2)$$

The Fourier transform of the matrix of force constants in the harmonic approximation is the dynamic matrix

$$D_{\alpha i,\,\beta j}(\mathbf{q}) = -\frac{1}{\sqrt{M_\alpha M_\beta}}\sum_{\mathbf{h}} Phi^{\mathbf{h}}_{\alpha i,\beta j}\exp[\mathrm{i}\mathbf{q}(\mathbf{h} + \boldsymbol{\tau}_\beta - \boldsymbol{\tau}_\alpha)] \qquad (3)$$

which defines the equation for normal modes or phonons

$$\sum_{\beta j}\left[D_{\alpha i,\,\beta j}(\mathbf{q}) - \omega^2\delta_{\alpha\beta}\delta_{ij}\right]\varepsilon_{\beta j}(\mathbf{q}) = 0 \qquad (4)$$

where M_α and M_β are the masses of atoms α and β, $\mathbf{h} = \mathbf{R}^0_m + \mathbf{R}^0_n$ is the direct lattice vector, $\delta_{\alpha\beta}$ and δ_{ij} are

Kronecker indices, ω and $\varepsilon_{\beta j}$ are the frequency and polarization of normal modes, respectively, which are determined by the wave vector $\mathbf{q}$ and the dispersion curve index λ.

In the application of lattice dynamics to a surface, it is necessary to take into account the disruption of the three-dimensional periodicity of the crystal along the direction perpendicular to the surface. This gives rise to additional modes on the surface that are missing in the crystal bulk. For the theoretical description of the surface dynamics, a crystal is often represented as having a surface as a film of finite thickness in which atomic planes are arranged parallel to the surface.[89] When the number of atomic layers in the film is large enough, most of atoms have environments corresponding to the coordination spheres in an ideal three-dimensional crystal; therefore, such films reproduce well the bulk properties. The atomic layers that confine the film simulate the free surfaces of the crystal. The film thickness is chosen in such a way that the force constants for atoms at the film centre are the same as in the bulk and the two opposite surfaces do not dynamically interact. On the film surface, there is translational periodicity, which is inherent in all film surfaces. The wave vector in this case forms a two-dimensional lattice in the plane (x, y) and dynamic matrix (4) is determined by the two-dimensional wave vector

$$\mathbf{q} = (\mathbf{q}_x, \mathbf{q}_y, 0)$$

For n atoms in the unit cell of the film, the dynamic matrix has dimensions $(3n \times 3n)$. Diagonalization of the Hermitian matrix for every value of the wave vector in the planar BZ affords $3n$ real non-negative eigen values $\omega^2(\mathbf{q},\lambda)$ corresponding to $3n$ values of the polarization eigenvectors $\varepsilon_{\beta j}$ $(\mathbf{q},\lambda)$, which are derived from Eqn (4). The normal modes of the film ($3n$) defined for every $\mathbf{q}$ can be classified according to their polarization and the squared displacement amplitude in different layers of the film. The character of localization of atomic vibrational amplitudes and the frequencies of surface phonons form the basis for their calculations in terms of the film model. All of the vibrational states of the film for the sets of points of the eigenvector $\mathbf{q}$ are thus calculated. Then the surface states are distinguished and classified according to polarization and frequency positions.

The method of representing the calculated phonon structure of the surface as dispersion curves along the symmetrical directions of the planar BZ is most popular due to its clearness and complete information coverage.[10] The dispersion curves of all states (except for those distinguished as surface states) form the location areas of bulk phonons and make it possible to easily follow the positions of the dispersion curves of surface phonons against the bulk states. As the film thickness increases, the number of surface phonon modes does not change and the number of bulk dispersion curves increases.

Two types of surface vibrational states are distinguished — true surface states and resonance states.[10] The true surface states are mainly localized in surface layers and can be located in forbidden gaps (energy bands forbidden for propagation of bulk vibrations), which are formed at the boundary of planar BZ as a projection of bulk vibrational states. In this case, the amplitude of atomic vibrations decreases exponentially toward the central layer of the film. The resonance states propagate in the bulk vibrational region; however, the displacement amplitude is maximum in the surface layers. When the wave vector $\mathbf{q}$ propagates along the symmetrical directions of the two-dimensional BZ, the vibrational modes are polarized either in the sagittal plane or in a plane in which all atoms shift perpendicularly to the plane. The atomic displacements are in this case of the plane-shift nature. For other directions of the propagation of vector $\mathbf{q}$, these two types of polarization are hybridized.

The effective potential [see Eqn (1)] is constructed using both *ab initio* methods[3,4] and semiphenomenological approaches.[32–34] In the *ab initio* calculations of the electronic energy of the ground state of the crystal, the density functional theory (DFT) has found wide use.[90,91] The essence of this approximation is that all properties of the electronic structure of the system in the non-degenerate ground state are fully determined by the electron density. The use of the DFT approximation to explore the bulk lattice dynamics is described in detail in the publication of Savrasov and Maksimov.[92] Reviews devoted to the application of DFT to describe the surface dynamics of semiconductors and metals were also reported.[3,4,93] However, as noted above, self-consistent *ab initio* calculations are highly time- and computation resource-consuming, especially in the case of systems with large numbers of atoms in the unit cell. It is more efficient to use model (semiempirical) methods, which take into account the many-particle nature of interatomic interactions inherent in metals and reproduce with good accuracy the bulk and surface properties.

2. Model many-particle potentials

Among semiempirical methods, most popular as applied to metals are DFT-based methods — EMT,[32] EAM[33] and TBA.[34] The difference between them is only in the procedure for description of electron density: in the case of EMT and EAM, this is the overall electron density created by the atomic environment at the location site of a given atom, while in the case of TBA, this is the width of the density of states function. A detailed description and comparison of these approaches was reported.[94] In this review, we give the results of calculations of surface phonons by means of the embedded atom method; therefore, we will describe in detail only this method.

The key idea of the EAM for the description of interatomic interactions proposed by Daw and Baskes[33] is that each atom, except for some chosen atom, is considered as an admixture to the system of the rest of atoms. The next basic statement is that the total electron density is well approximated by the linear superposition of the contributions of separate atoms. The theoretical substantiation of the EAM within the framework of the local density approximation (LDA) carried out in two publications[95,96] demonstrated that the EAM is valid for metals with electron density adequately described by a superposition of atomic densities (simple sp metals and metals with almost fully occupied d-shell).

In terms of the EAM, the configurational energy of the metal determined with respect to the sum of energies of free atoms is expressed by two contributions

$$E = \sum_i F_i(\bar{\rho}_i) + \frac{1}{2}\sum_{ij}{}' \Phi_{ij}(R_{ij}) \qquad (5)$$

The first term reflects the energy benefit caused by embedding the given atom into the electron density created by a superposition of all other atoms at the location site of the chosen atom. The second term is the sum of pair potentials describing the repulsion of two shielded ions. Here $F_i(\bar{\rho}_i)$ is the energy of embedding of atom i as a function of local density, $\bar{\rho}_i$, $\Phi_{ij}(R_{ij})$ is the pairwise interaction potential of atoms i and j located at distance R_{ij}; the prime mark at the summation sign implies the absence of items with $i = j$.

The local electron density is determined by the superposition of atomic densities $\rho_i^{\mathrm{a}}(R)$

$$\bar{\rho}_i = \sum_{i \neq j}' \rho_j^{\mathrm{a}}(R_{ij}) \tag{6}$$

The atomic densities $\rho_j^{\mathrm{a}}(R)$ can be derived from the solution of the atomic problem for a neutral atom in the LDA approximation.[90] In this case, the atomic densities are set equal to the electron density of the outer-shell electrons

$$\rho^{\mathrm{a}}(R) = n_{\mathrm{s}}\rho_{\mathrm{s}}^{\mathrm{a}}(R) + (n - n_{\mathrm{s}})\rho_{\mathrm{p}}^{\mathrm{a}}(R) \tag{7}$$

where n is the number of outer-shell electrons, n_{s} is the number of outer-shell s electrons $\rho_{\mathrm{s}}^{\mathrm{a}}$, $\rho_{\mathrm{p}}^{\mathrm{a}}$ are the densities related to wave functions of s and p electrons.

The charge density of the metal atom is calculated from the configuration of the valence electrons. The selection of the formula for the pair potential was discussed.[97] It was concluded that it is admissible to express the pairwise interaction potential of shielded ions in a metallic conducting medium in the following form:

$$\Phi_{ij}(R) = \frac{Z_i(R)Z_j(R)}{R} \tag{8}$$

where

$$Z(R) = Z_0(1 + \beta R^{\nu})\exp(-\alpha R) \tag{9}$$

Z_0 is the number of outer-shell electrons; for reproducing the elastic characteristics of the metals, the parameter ν was taken to be 1 or 2, β and α are free parameters.[33]

In the case of a monoatomic system, the configurational energy described by Eqns (5)–(9), with known embedding energy $F(\bar{\rho})$, as a function of the local density $\bar{\rho}$ depends on only two free parameters α and β. In the works,[95,96] the embedding function $F(\bar{\rho})$ was constructed using the universal equation of state (Refs 98 and 99) expressed by empirical formula relating the sublimation energy (E_{sub}) to the characteristic linear dimension of the crystal lattice (the lattice constant a for FCC and BCC lattices)

$$E_{\mathrm{sub}} = E_0(1 + a^*)\exp(-a^*) \tag{10}$$

where E_0 is the sublimation energy at the equilibrium value of the lattice constant $a = a_0$;

$$a^* = \frac{a/a_0 - 1}{(E_0/9B\Omega)^{1/2}}$$

B is the bulk modulus of elasticity, Ω is the crystal volume per atom.

The equation of state (10) adequately describes experimental volume *vs.* pressure dependences at low temperatures for some metals with close-packed cubic structures, including FCC transition metals.[98] This justifies the use of the given formula together with formula (5) for the construction of the embedding function $F(\bar{\rho})$. The selection of experimental information for determination of the fitting parameters used in the EAM was considered and substantiated by Foiles.[97] The parameters α and β of Eqn (9) were fitted to the experimental values of the sublimation energy, elastic constants, equilibrium volume and the energy of vacancy formation in the metals being studied (the fitting was performed to experimental data used in Ref. 96). The calculated bond energy, lattice constant and bulk modulus B for each metal upon the use of the universal equation of state (10) exactly reproduce the experimental values at any variation of the adjustable parameters α and β.

For a non-monoatomic system, the pair potential has the form of a screened Coulomb potential and is used in the form proposed by Johnson [100]

$$\Phi_{AB}(R) = \frac{1}{2}\left[\frac{\rho_B(R)}{\rho_A(R)}\varphi_A(R) + \frac{\rho_A(R)}{\rho_B(R)}\varphi_B(R)\right] \tag{11}$$

where φ_A and φ_B are pair potentials and ρ_A and ρ_B are the charge densities of the substrate and the adsorbate, respectively.

Table 1. Lattice constants (a_0), sublimation energies (E_{sub}), elastic constants (C_{11}, C_{12}, C_{44}) and vacancy formation energies (E_{v}) for pure metals that we used to construct the interatomic interaction potentials.[95]

Parameter	Cu	Ag	Al	Ni	Pd	Li	Na	K
a_0 /Å	3.61	4.09	4.08	3.52	3.89	3.51	4.21	5.23
E_{sub} /eV	3.54	2.85	3.93	4.45	3.91	1.63	1.11	0.94
C_{11} /erg cm^{-3}	1.68	1.21	1.84	2.33	2.28	1.45	0.87	0.46
	1.70 [a]	1.24 [a]	1.86 [a]	2.46	2.34 [a]	1.48 [b]	0.86 [b]	0.45 [b]
C_{12} /erg cm^{-3}	1.23	0.96	1.58	1.51	1.81	0.11	0.78	0.37
	1.22 [a]	0.93 [a]	1.57 [a]	1.47 [a]	1.76 [a]	0.11 [b]	0.79 [b]	0.36 [b]
C_{44} /erg cm^{-3}	0.76	0.46	0.43	1.28	0.76	0.11	0.59	0.26
	0.75 [a]	0.46 [a]	0.42 [a]	1.24 [a]	0.71 [a]	0.10 [b]	0.58 [b]	0.25 [b]
E_{v} /eV	1.31	1.09	0.88	1.55	1.37	0.34	0.42	0.34
	1.3 [a]	1.1 [a]	0.9 [a]	1.6 [a]	1.4 [a]	0.34 [b]	0.41 [b]	0.34 [b]

[a] From Ref. 96. [b] From Ref. 101.

The experimental data on the dispersion curves of the phonon spectrum (except for the long-wavelength region, which determines the elastic constants) were not included in the constructed potentials. Due to this circumstance, it is possible, on the one hand, to perform additional testing of the constructed potentials by comparing the calculated and experimental phonon dispersion curves; on the other hand, this increases the reliability of the calculated surface phonons for which experimental information is missing or scattered. This seems to be especially important for the potentials used for theoretical investigation of atomic vibrations in intricate objects such as vicinal surfaces of metals and surface structures. The experimental [101] and calculated [96] values of the characteristics employed to construct the potentials of interatomic interactions are presented in Table 1. Thus, using EAM it is possible to reproduce with good accuracy some experimentally determined characteristics of metals by varying only two fitting parameters.

IV. Results of investigations of surface phonons

A necessary condition for the description of the dynamics of a metal surface is the structural optimization of the atomic configuration, *i.e.*, consideration of the surface relaxation. The relaxation of the metal surfaces with different crystallographic orientations was studied in detail both experimentally [102–108] and theoretically;[4, 61, 62, 108–110] therefore, we do not dwell on this issue here. Note only that the results of calculations of the relaxation of both simple and vicinal surfaces of the considered metals carried out using EAM interatomic interaction potentials are consistent with experimental data [101–107] and *ab initio* calculations.[109–113]

The adequacy of using EAM potentials for the study of phonons on surfaces having steps and adatoms is verified by comparing the dispersion curves calculated for the bulk material and for ideal and relaxed simple surfaces with results of experiments [114] and *ab initio* calculations.[115]

1. Phonons on low Miller index metal surfaces

The bulk dispersion curves along symmetrical directions of the BZ for sodium and copper calculated using the EAM potentials are shown in Fig. 1. It can be seen that EAM potentials reproduce with good accuracy the long-wavelength region of the bulk spectra. The deviations are present only near the BZ boundary. For alkali and noble metals, the deviation from the experimental data does not exceed 3%. The greatest deviations of $\sim 7\% - 10\%$ are inherent in FCC d transition metals. These deviations are due to the method used to construct the potentials of interatomic interactions.[33] When determining the fitting parameters of the potentials, experimental data on the elastic constants are used; this reflects information only on long-wavelength atomic displacements with a wave vector in the central area of the BZ. The lack of information on short-wavelength phonons in the fitting parameters additionally attests to the good quality of EAM potentials.

For calculation of the phonon structure of simple clean metal surfaces and adsorption structures on these surfaces, a film consisting of 31 atomic layers is chosen. In the case of vicinal surfaces, the film thickness varies from 45 to 72 atomic layers depending on the surface geometry. This thickness is sufficient to exclude the interference of vibrations from the opposite surfaces of the film and to obtain bulk phonons in the central part.

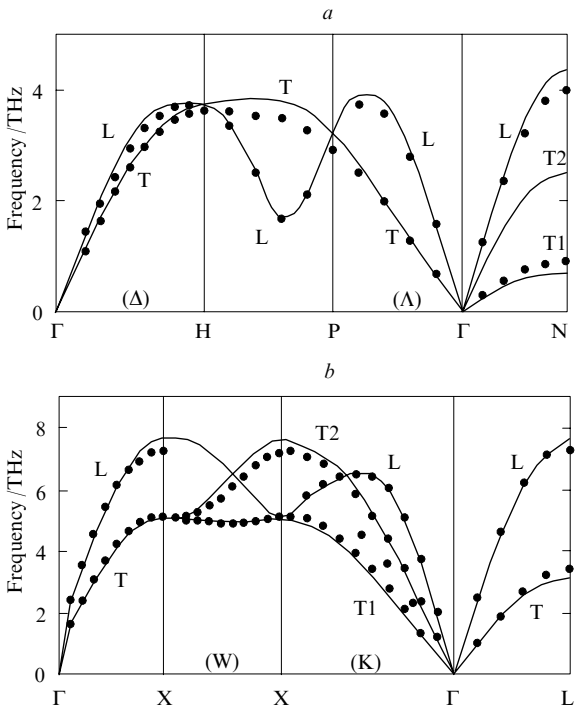


Figure 1. Dispersion curves of bulk phonons along the [001], [011] and [111] directions of the BCC lattice of sodium (*a*) and FCC lattice of copper (*b*).
L, T, T1, T2 are bulk modes; the dots correspond to experimental data; the curves show the EAM calculation data.[61]

Detailed analysis of the experimental results and *ab initio* calculations on simple surfaces for a number of FCC metals was reported in a review.[4] The results of EAM calculations of the phonon spectra of simple Al, Li, Na, Cu, Ag and Pd surfaces are presented in several works.[43, 45, 46, 116–123] Comparison of the EAM calculation results with experimental [13–22, 124–126] and theoretical [44, 127–133] data demonstrated excellent agreement. Using the EAM, it was possible to describe in detail the acoustic longitudinal resonance arising on all surfaces of these metals, which is located near the lower boundary of bulk vibrations and corresponds to the displacements of atoms in the sagittal plane (*yz*-polarization). A specific feature of this resonance is the abnormally low frequency of longitudinal vibrations (lower than the frequency of transverse vibrations), whereas the longitudinal vibration branch in the bulk spectrum is located much higher than the transverse vibration branches. At low values of the wave vector **q**, the acoustic resonance penetrates into the region of bulk vibrations and only near the BZ boundary it acquires the surface character.

This vibrational state was detected experimentally for the first time using the HAS and EELS methods on simple surfaces of almost all FCC metals.[14, 15, 21, 124] It was impossible to describe the nature of the acoustic longitudinal resonance within the framework of a simple force constant model,[127] because it is impossible to take into account the structural relaxation of the surface. On the basis of the

model EAM calculation of ideal and relaxed simple surfaces of FCC metals (Al, Ni, Cu, Ag, Pd, Pt) and analysis of the variation of the surface force constants, a correlation was established between the relaxation and the change in the force constants in the surface atomic layer, on the one hand, and the character of surface dispersion curves on the other hand.[134] The relaxation in the indicated metals enhances interlayer interactions and weakens the interactions within the surface layer.[134] For both types of interaction, this factor becomes more pronounced with decreasing surface packing density and increasing atomic mass and is most significant for d transition metals (Pd, Pt). A study of the phonon spectra of the ideal and relaxed surfaces ascertained that the character of atomic interactions in the surface layers changes upon structural relaxation of the surface, and low-frequency longitudinal resonance appears. Force constant analysis demonstrated that the longitudinal resonance is caused by the interatomic interaction in the surface layer and is especially pronounced in the vibrational spectra of metals having large atomic mass for which the transverse interactions are considerably weakened.

The phonon spectra of Al(111) and Pd(111) surfaces calculated using EAM potentials[43, 121] are presented in Fig. 2. The calculation for aluminium and palladium surfaces demonstrated that due to relaxation, the interactions within a layer are weakened by 10% and 50%, respectively. This results in a decrease in the energy of the longitudinal resonance (LR) mode. For Al(111), the LR mode is located at the edge of the projection of bulk phonons and is mixed with them (see Fig. 2 *a*). In the case of Pd(111), the LR mode is split from bulk vibrations and has clear-cut surface character in the symmetrical point $\overline{\mathrm{K}}$ located at the BZ border (see Fig. 2 *b*).

A EAM calculation[119] also identified a high-frequency resonance in the $\overline{\Gamma}$ point on the (110) surface of FCC metals, this resonance being formed by coupled vibrations of the first- and second-layer atoms polarized along the direction strictly perpendicular to the surface. In early experiments, this resonance was not detected, probably because of the fact that helium atoms in the HAS method are scattered by oscillations of the surface electron density by $\sim 2-3$ Å distances from the first atomic layer. This mechanism of helium atom scattering is suitable for detecting only displacements of first-layer atoms parallel to the surface.[15] However, for the (110) surface considered, it is significant to take into account the vibrations of second- and even third-layer atoms, because it is prone to multilayer and alternating-sign relaxation. With increase in the resolution of the HAS and EELS experimental methods, similar high-frequency resonances were detected for silver, nickel, copper and palladium (110) surfaces.[15, 135–138] Indeed, on the Pd(110) surface, which is characterized by markedly shortened first interlayer spacing ($\Delta_{12} = -8.3\%$), the resonance was detected experimentally[22] at 16.80 meV. This value is consistent with the data of EAM calculation (16.34 meV), whereas the *ab initio* calculation for Pd(110) afforded an overestimated value for the energy of this resonance (18.1 meV).[4]

Generally, the phonon spectra of simple surfaces of FCC metals with the same atomic geometry are similar (see Fig. 2). They always contain a Rayleigh mode, and in the short-wavelength limit (large wave vector **q**), this mode is located below the bottom of the projection of bulk phonons and is of the clear-cut surface nature. At small **q** (long-wavelength limit), the Rayleigh mode penetrates deep

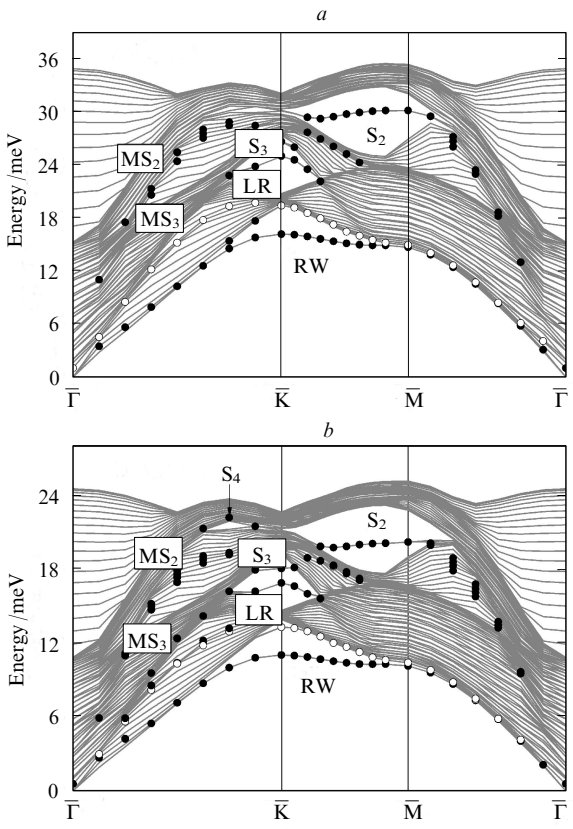


Figure 2. Dispersion curves of phonons of relaxed 31-layer Al(111) (*a*) and Pd(111) films (*b*) along symmetrical directions of the planar BZ.[43, 45]
The surface states are designated by dots; LR is longitudinal resonance (light dots); RW is the Rayleigh wave, S_2, S_3, S_4 are longitudinal gap modes, MS_2, MS_3 are resonance modes. The surface modes are designated according to the classification presented in Refs 10 and 11. Here and in other figures, the subscript numerals correspond to the number of those layers the displacements of whose atoms make the largest contributions to the vibrational mode.

into the bulk and, being coupled with bulk vibrations, becomes a resonance that is polarized in the sagittal plane. In the short-wavelength region where the bulk vibrations are forbidden (forbidden gap), there always exist surface vibrational states with longitudinal polarization caused by displacement of atoms of the two first layers parallel to the surface. Along the directions from the BZ centre to boundary, surface resonances resulting from coupled vibrations of surface and bulk atoms are always detected. The vibrational spectra of FCC metals differ by the energies of the surface vibrational states and the degree of localization of these states in the surface layer. The general influence of the surface relaxation on the phonon spectra of simple surfaces of FCC metals is manifested as a high-frequency shift of the transverse and low-frequency shift of the longitudinal surface modes. Furthermore, relaxation gives rise to a new surface vibrational state with the longitudinal-shear polarization, which has a resonance nature at the planar BZ boundary for metals such as Al, Cu and Ni and clear-cut surface nature for Ag, Pd and Pt. Presumably, the presence of exactly this mode and its 'softening' determine the phonon contribution to the structural rearrangement of the simple surfaces of some FCC metals (*e.g.*, Pd and Pt).

In the case of BCC alkali metals, experimental values for surface phonon relaxation and dispersion were found only for sodium and potassium.[125, 139, 140] Theoretical data for these metals were obtained by using the parameterized force constant method [36] and *ab initio* calculations.[125, 140, 141] This enables testing of the EAM potentials and verification of the reliability of calculation results when considering the alkali metal adsorption on the surface of FCC metals.

The optimization of the atomic structures of the alkali metal (100) and (110) surfaces in the EAM approximation demonstrated that the interlayer spacings increase.[48, 120, 122] For example, the changes in the interlayer spacings Δ_{12}, Δ_{23} and Δ_{34} for the Na(110) surface are +2.4%, +0.1% and +0.6%, respectively. As in the case of FCC metals, a decrease in the surface packing density induces enhancement of relaxation effects. For the Na(100) surface, the Δ_{12}, Δ_{23} and Δ_{34} values are +8.6%, +0.7% and +0.1%, respectively. The surface relaxation also increases with increase in the lattice parameter and the atomic mass, for example, on going from lithium to potassium. However, in only one experiment,[139] was minor decrease in the first interlayer spacing, $\Delta_{12} = -0.3 \pm 0.3\%$, detected for the Na(110) surface. The same relaxation pattern for the Na(110) surface results from *ab initio* calculation.[141] The differently directed Δ_{12} values in *ab initio* and EAM calculations may be due to the use of different atomic configurations in the construction of interatomic potentials. However, since the energy difference between the relaxed and ideal surfaces does not exceed 1%, this does not make a noticeable contribution to the phonon spectrum.[120, 122] Detailed description and analysis of the phonon spectra for sodium and lithium (100) and (110) surfaces were reported;[48, 120, 122, 125] therefore, we restrict ourselves to considering the phonon spectra for similar potassium surfaces.

The dispersion curves obtained in the EAM approximation are presented in Fig. 3. Characteristic features of the phonon spectra of potassium are very low vibrational frequencies of surface atoms and high density of resonance states with shear-planar or shear-vertical polarization in the sagittal plane. Only at the boundary of the planar BZ, are true surface states, *i.e.*, Rayleigh modes, are manifested. Note that EAM calculation on the K(100) surface reproduces the vibrational mode that propagates along the $\bar{X}\bar{M}$ direction and is located at the boundary of the bottom of the bulk phonon projection. This mode is largely degenerate with bulk vibrations and is mainly localized in the first three surface layers the atoms of which vibrate in the sagittal plane. It is believed that the presence of this shear mode is typical of the (100) surfaces of all BCC metals.[37] Good quantitative agreement of the EAM-calculated energy of the shear mode at the $\bar{X}$ point and *ab initio* calculation results is observed,[140] namely, 4.30 and 4.71 meV, respectively. Comparison with the phonon spectra of the corresponding surfaces of sodium and lithium demonstrated that the phonon spectra of all alkali metals are qualitatively similar.[36, 120, 125, 140] As in the case of FCC metals, the difference is only in the vibrational state energies and degrees of localization on a particular surface layer.

Force constant analysis for relaxed Li(110) and Na(110) surfaces demonstrated that the intralayer interaction in the surface layer is enhanced (by ~3%–6%), while the interlayer interaction weakens (by 25%–30%) as compared with the corresponding interactions in the bulk. As the lattice parameter and the metal atomic mass increase, the interlayer force constants decrease to even a greater extent (for potassium, the decrease is 45%). The intralayer interaction (it is stronger than the interlayer interaction) can lead to shear of the surface layer in the direction parallel to the surface. Thus, presumably, due to weakening of the interlayer interaction, increase in the density of shear modes and decrease in the frequency of alkali metal (100) and (110) surfaces in the phonon spectrum, these surfaces become dynamically unstable to shear displacements. This is confirmed by the low-temperature martensite-type structural transition occurring in alkali metals. For example, lithium tends to transform from BCC to 9R structure, while sodium has a BCC to HCP transition [48, 122] along the (110) plane.

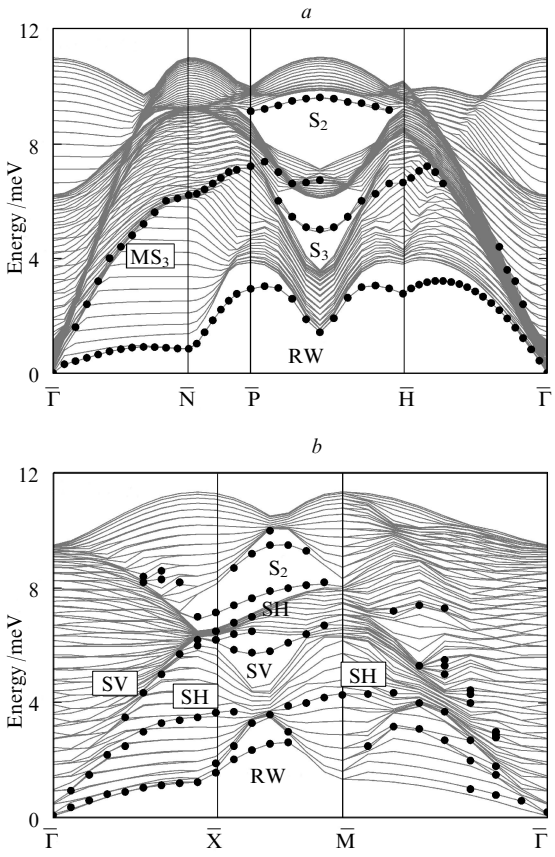


Figure 3. Dispersion curves of phonons in relaxed 31-layer K(110) (*a*) and K(100) films (*b*) along symmetrical directions of the planar BZ.[134]
SV is the shear vertical mode, SH is the shear horizontal mode.

2. Phonons on high Miller index metal surfaces

The geometric model of the vicinal surface can be represented as a section of a bulk lattice by a high Miller index plane at a small angle to a low-index plane. These surfaces consist of equally wide terraces formed by ideal planes with low Miller indices separated by regularly arranged monoatomic steps. As the size of the terraces increases, the normal vector to the vicinal surface approaches the normal vector to the terrace.† The corresponding angles (φ) between the

† This is the reason for the surface name 'vicinal' (from Latin *vicinus*), *i.e.*, nearly close packed.

Table 2. Classification of vicinal surfaces with close-packed terrace and step planes.[59]

Class	Miller index	Terrace/step plane	φ /deg	Step edge direction	BZ type
A	(211)	3(111) × (100)	19.50	[01$\bar{1}$]	simple rectangular
B	(311)	2(100) × (111)	25.24	[01$\bar{1}$]	centred rectangular
	(511)	3(100) × (111)	15.80	[0$\bar{1}$1]	the same
C	(331)	3(111) × (111)	22.00	[$\bar{1}$10]	"
	(221)	4(111) × (111)	18.24	[$\bar{1}$10]	simple rectangular

normals for different classes of vicinal surfaces are summarized in Table 2.

The classification of vicinal surfaces in terms of Miller indices evidently does not reflect the atomic structure of the plane. A more vivid notation was proposed by Lang *et al.*[142] The structure of the vicinal surface in this case is given by

$$m(h_t k_t l_t) \times n(h_s k_s l_s)$$

where m is the width of the terrace with orientation $(h_t k_t l_t)$ determined by the number of atomic rows parallel to the step edge on the terrace; n is the height of the step with orientation $(h_s k_s l_s)$, which is equal to the number of atomic diameters. For example, the notation 2(111) × 1(100) means that the vicinal (211) surface has (111) terraces with a width of two atomic rows and (100) step with a height of one atom. For FCC metals, surfaces in which the step-edge atoms occur at the first coordination sphere distance from the neighbouring terrace atoms located in the step corner are energetically most favourable. These steps may occur in the (100) or (111) planes. The model of an FCC crystal confined by a vicinal (211) surface and the relaxation displacements of surface atoms are shown in Fig. 4. Lower symmetry of vicinal surfaces results in larger surface unit cell. The unit cell of the (211) surface comprises two terrace atoms and one step-edge atom (see Fig. 4 *b*).

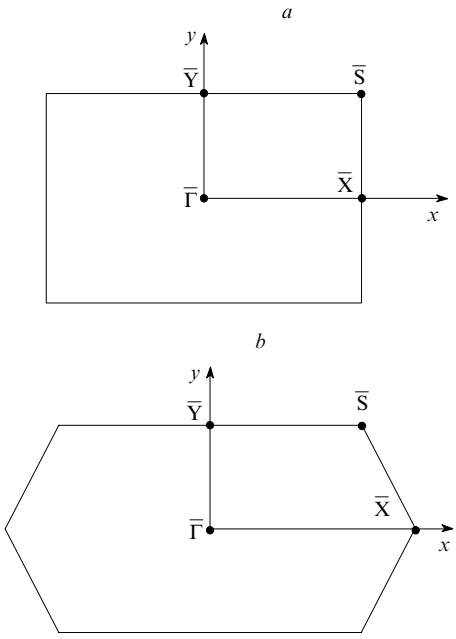


Figure 5. Two-dimensional Brillouin zones of vicinal surfaces of FCC metals: (110), (211), (221) (*a*) and (311), (331), (511) (*b*).[47]

Depending on the structure (geometry), the two-dimensional BZ of vicinal surfaces may be either simple rectangular or centred rectangular, being determined by the size and symmetry of the planar unit cell. The Brillouin zones of the vicinal surfaces are shown in Fig. 5.

The above-described geometry of the vicinal surfaces corresponds to an ideal crystal. A description of the surface dynamics has to take into account the relaxation. By now, the relaxation of the vicinal surfaces of copper has been studied most comprehensively; the (211), (311), (511), (711), (331), (210) and (310) surfaces were studied both theoretically[44,47,60–62,143–149] and experimentally.[108,150–155] For vicinal surfaces of copper, (911), (221), (551), (310), (410), (510), (710), (910), (332), (553), (775) and (443), only theoretical calculations (both model and *ab initio*) are available.[44,60,62,63,146–149] This is due to the sensitivity of

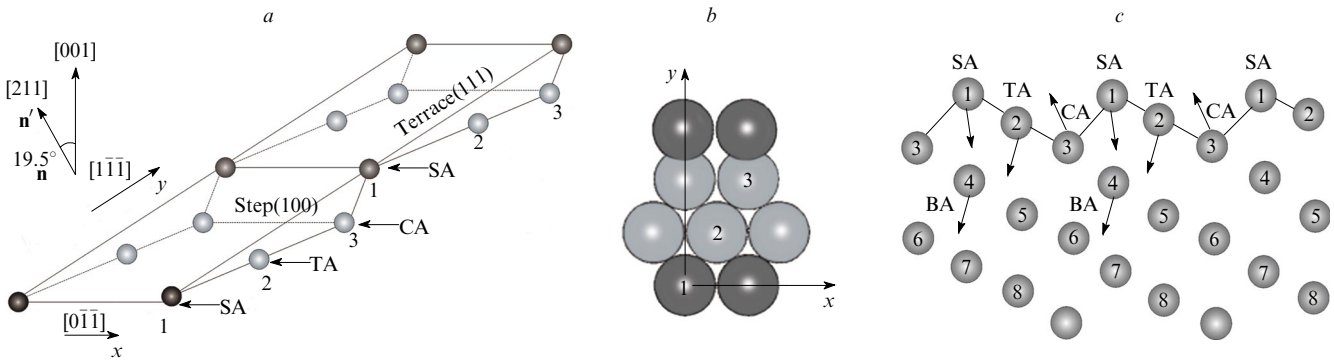


Figure 4. Structure (geometry) of the (211) vicinal surface (*a*), its unit cell (*b*) and relaxation displacements of surface atoms (*c*).[134] SA is the step atom, TA is the terrace atom, CA is the atom located in the corner formed by the step and the terrace, BA is the nearest bulk atom. Digits 1–8 designate atoms of the corresponding atomic layers.

experimental methods,[152] which are unsuitable for describing relaxation of surfaces with interlayer distance of < 1 Å. The relaxation of the palladium (210), (320), (430), (211), (511) and (331) vicinal surfaces has been studied in considerable detail (mainly theoretically).[47, 155, 156] Data on the relaxation of vicinal surfaces of other FCC metals are disembodied, and only for some surfaces, either experimental or theoretical data were reported: Al(210), Al(311), Al(331);[47, 112, 157–161] Ni(311),[162] Ni(977),[112, 163] Ag(410).[47, 112, 164–166] Note rather pronounced discrepancies of both experimental and theoretical data on the relaxation of vicinal surfaces. Indeed, the changes in the second interplanar spacing Δ_{23} found by LEED[153, 154] and X-ray diffraction[153] for the Cu(511) surface are -6.1% and $+8.1\%$, respectively. Upon the use of one and the same full-potential linear augmented plane wave (FLAPW) method, different authors[147, 164] obtained Δ_{12} values for the Cu(511) surface of -11.2% and -22.1%, respectively.

Since the most complete information on surface relaxation is available for copper vicinal surfaces (Table 3), we will illustrate the adequacy of using EAM potentials in relation to relaxation of the vicinal surfaces of this FCC metal. For the (211), (311) and (511) surfaces, a clearly defined correlation can be followed between the relative change in the interlayer spacing and the number of atoms that form the terrace. The number of upper layers that are compressed is most often equal to the number of atoms on a terrace (N). With increase in the serial number of the interlayer spacing, every $(N+1)$th interlayer spacing increases. The pattern of sign alternation of the relaxation is still retained for deeper atomic layers.

Comparative analysis of the relaxation of vicinal surfaces for the FCC metals in question (Al, Cu, Ni, Ag, Pd, Pt) indicated that the qualitative multilayer relaxation pattern is determined to a large extent by the number of atoms that form the terrace of the particular surface. In most cases, the number of upper atomic layers that are compressed coincides with the number of terrace atoms. The cases where this is not true can be attributed to local influence of the step on the relaxation of atoms located near the step. This statement is validated unambiguously by invariability of the deviation of the number of upper atomic layers being compressed from N following increase in the terrace size. The chemical nature of a particular element is manifested most clearly in the step. The value of relaxation of vicinal surfaces generally tends to increase for heavier FCC transition metals. Comparison with the data of other calculations and experiments showed agreement for the EAM potentials used (they reproduce both the sign and the value of relaxation).

The formation of a step (linear defect) on the surface gives rise to a new type of coupled vibrations of atoms with the amplitude being located on the step (step mode).[58, 59, 167] The new type of vibrations can be better conceived by drawing analogy with the surface phonons. The existence of surface phonons is due to the appearance of a two-dimensional defect, a free surface, in the crystal. The surface phonon propagates over the surface and does not penetrate deep into the bulk. By analogy with the surface phonon, the step mode propagates only along the step and does not get in the terrace. The energy of the step mode is transferred to the terraces and into the crystal bulk upon interaction with surface and/or bulk phonons. The possibility for the step mode to propagate only along the step is limited by the direction of its wave vector (step modes can exist only along one direction of the surface BZ, which coincides with the direction along the step). The vibrational spectra of vicinal surfaces are most often simulated in the thin film model. The orthogonal coordinate axes are chosen in such a way that the x-axis is directed along the step for all surfaces and corresponds to the reciprocal space direction $\overline{\Gamma}\,\overline{X}$. The phonon spectra of vicinal surfaces of various classes found in the EAM approximation are shown in Figs 6–8. The

Table 3. Change in the distances Δ_{ij} between the surface atomic layers i and j of copper (in percent relative to the bulk interlayer spacing).

Surface	Method	Δ_{12}	Δ_{23}	Δ_{34}	Δ_{45}	Δ_{56}	Δ_{67}	Δ_{78}	Ref.
Cu (211)	EAM	−10.3	−5.1	+7.3	−5.6	−1.1	+3.7	−2.5	47
	DFT	−12.2	−9.5	+8.7	−2.1	−1.6	+1.5	−0.1	61
	DFT	−14.4	−10.7	+10.9	−3.8	−2.3	+1.7	−1.0	62
	LEED	−14.9	−10.8	+8.1	–	–	–	–	150
Cu (311)	EAM	−8.9	+3.8	−3.6	+2.0	−1.3	+0.8	–	47
	FLAPW	−12.9	+4.2	−0.6	+0.2	+0.4	–	–	146
	LEED	−7.3	+3.7	0.0	–	–	–	–	167
	LEED	−11.9	+1.8	–	–	–	–	–	149
Cu (511)	EAM	−9.5	−7.4	+8.7	−4.2	−3.8	+4.6	−1.6	47
	DFT	−9.3	−10.7	+7.2	−2.9	+1.1	+1.7	−1.5	61
	FLAPW	−10.5	−9.8	+6.2	−4.3	+2.8	+1.3	−2.3	146
	LEED	−13.2	−6.1	+5.2	−0.1	+2.7	−3.1	−3.3	151
	X-ray	−15.4	+8.1	−1.1	−10.3	+5.4	−0.7	−6.9	153
Cu (331)	EAM	−10.5	+2.0	−1.5	−0.4	−0.2	–	–	47
	DFT	−12.7	−3.3	+4.5	−2.0	+0.1	−0.1	+0.8	61
	FLAPW	−12.3	−3.1	+5.2	−2.5	+0.6	+0.6	+0.1	147
	FLAPW	−22.0	+1.6	+6.9	−2.4	−0.6	−0.4	–	148
	LEED	−13.8	+0.4	+4.0	−4.0	–	–	–	151
Cu (221)	EAM	−10.9	−6.8	+6.0	−1.0	−5.4	+2.6	+1.0	47
	FLAPW	−15.1	−4.4	−1.1	+6.2	−5.3	−0.4	+2.1	146

Note. Negative (positive) Δ_{ij} implies compression (expansion) of the interlayer space.

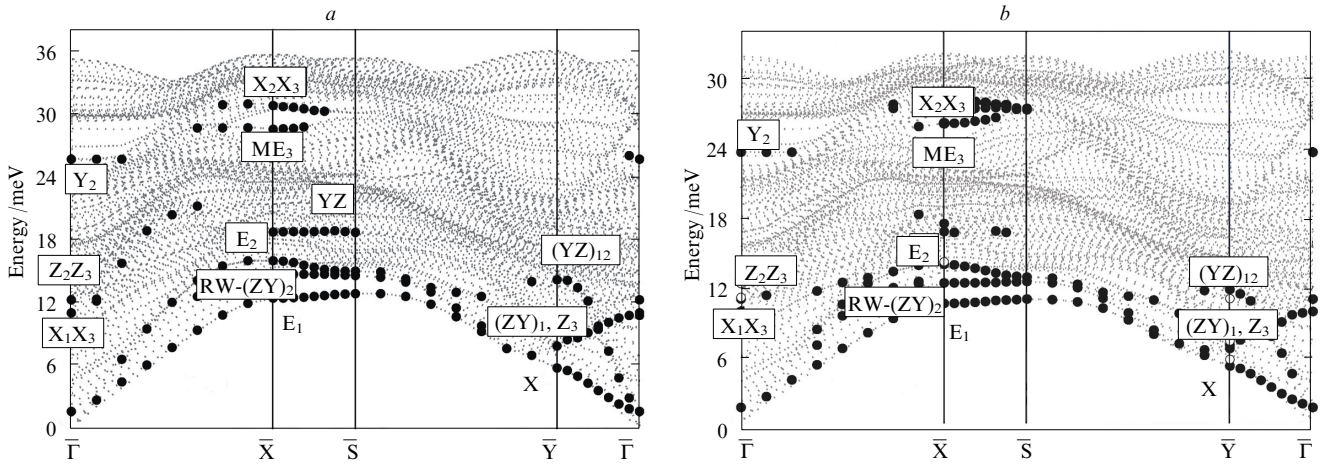


Figure 6. Dispersion curves of phonons of relaxed 48-layer Al(211) (*a*) and Cu(211) films (*b*).[47]
The surface modes are designated according to Knipp classification.[59] The polarization atomic displacements X, Y, Z coincide with the [0$\bar{1}$1], [$\bar{1}$11] and [211] directions, respectively.

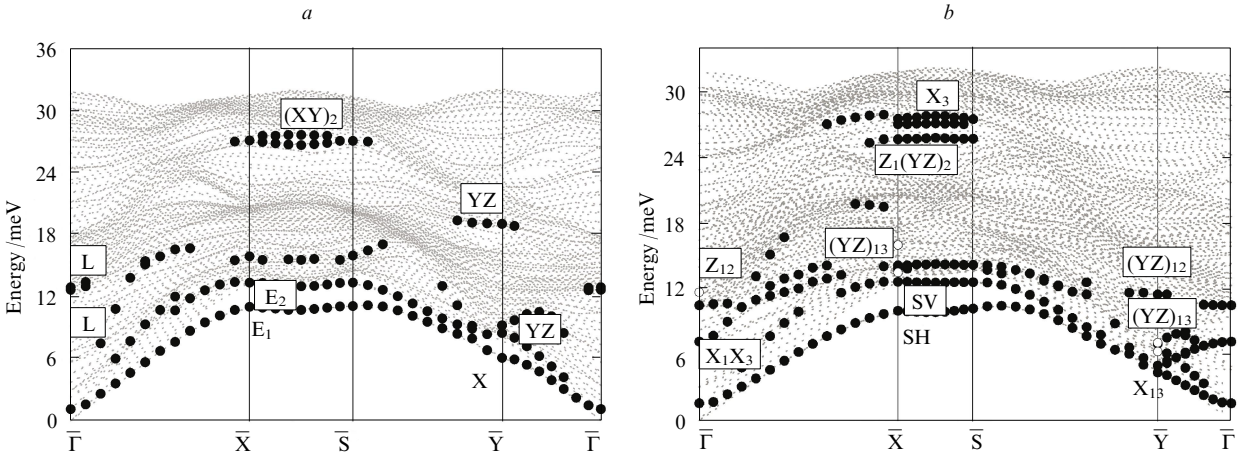


Figure 7. Dispersion curves of phonons of relaxed 45-layer Cu(331) film (*a*) and 81-layer Cu(511) film (*b*).[47]
The polarization atomic displacements X, Y, Z coincide with the [0$\bar{1}$1], [$\bar{2}$33], [311] (*a*) and [0$\bar{1}$1], [$\bar{2}$55], [511] (*b*) directions, respectively.

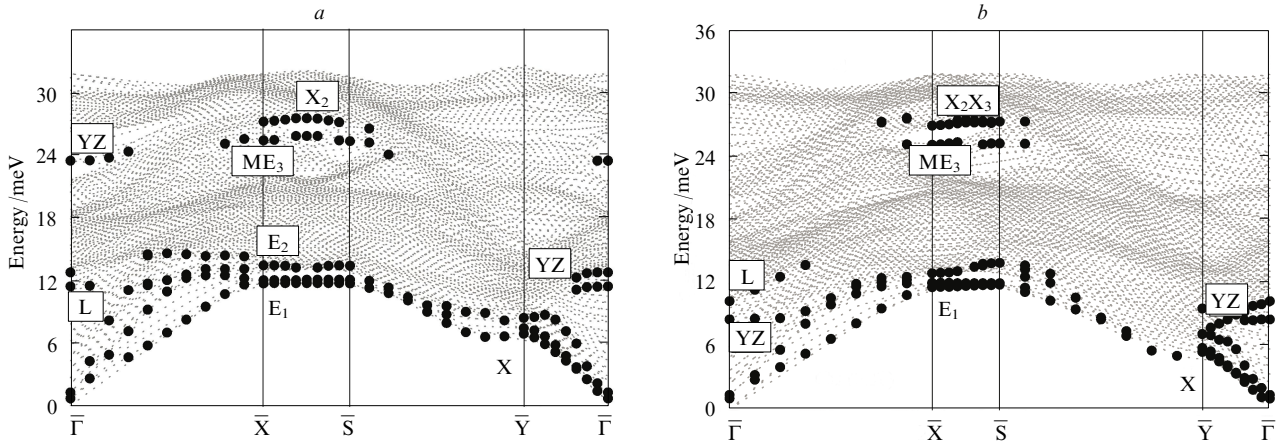


Figure 8. Dispersion curves of phonons of relaxed 57-layer Cu(331) film (*a*) and 72-layer Cu(221) film (*b*).[47]
The polarization atomic displacements X, Y, Z coincide with the [$\bar{1}$10], [$\bar{1}\bar{1}$6], [311] (*a*) and [$\bar{1}$10], [$\bar{1}\bar{1}$4], [221] (*b*) directions, respectively.

spectra are presented for two FCC metals, copper and aluminium, which are subsequently considered as the substrates for the sub-monolayer adsorption of alkali metals. According to the classification of the possible polarizations of step modes on vicinal surfaces with close-packed terraces and steps [(111) or (100)] proposed by Knipp,[59] there are three step modes, two transverse and one longitudinal modes, which are designated by E_1, E_2 and ME_3, respectively. The mode E_1 has the lowest frequency and is located below the Rayleigh mode. The mode E_2 occurs near the lower edge of the bulk vibrational frequency but above the Rayleigh mode. The high-frequency longitudinal mode ME_3 is always coupled with the bulk states.[59]

The effect of relaxation on the phonon structure of vicinal surfaces was analyzed by comparing the spectra of ideal and relaxed films of all considered FCC metals. The relaxation is critical for the step modes located at the boundary of bulk vibrations, because it induces either increase or decrease in their energy. As this takes place, either step modes lose their localized nature being mixed with bulk vibrations or surface modes that are split from the bulk phonon spectrum appear. In the general case, relaxation leads to an increase in the energy of transverse and longitudinal shear modes (by $\sim 0.4-1.2$ meV) and virtually does not influence the energy of longitudinal modes propagating in the surface plane.

a. Phonon spectra of class *A* vicinal surfaces

The (211) surface refers to class *A* and is formed by terraces in the (111) plane and steps with (100) orientation. The dispersion curves for relaxed Al(211) and Cu(211) surfaces are presented in Fig. 6. The phonon spectra of both metals were found to display typical step modes.[59] The most pronounced surface nature of the step modes is seen at the BZ boundary. Consider the $\overline{\Gamma}\,\overline{X}$ and $\overline{\Gamma}\,\overline{Y}$ directions corresponding to the directions along the step and normal to the step. Along the $\overline{\Gamma}\,\overline{X}$ direction, the Rayleigh mode and the step modes E_1 and E_2 are manifested.

At the $\overline{X}$ point, the lower mode related to transverse vibrations of atoms located on the step and below the step is the mode E_1. The displacements of step atoms mainly occur in the (211) plane. This state is ($\sim 50\%$) localized in the first and third layers. As the wave vector decreases, the mode E_1 gets into the region of bulk vibrational states and becomes a resonance. Simultaneously, the degree of localization on the step decreases, while the penetration depth into the bulk increases. The second lowest state localized ($\sim 70\%$) on the terrace atoms is the Rayleigh mode of the (111) surface a fragment of which is the terrace. The third state at the $\overline{X}$ point is the step mode E_2 caused by vertical displacements of atoms localized ($\sim 85\%$) on the step. When the wave vector decreases, all three modes lose rather rapidly the surface character and at $\mathbf{q}_x \approx 0.75|\overline{\Gamma}\,\overline{X}|$, they already become resonances. The lower mode on the forbidden gap (point $\overline{X}$) is the step mode ME_3 corresponding to the longitudinal displacements of the step atoms and corner atoms. The two upper gap states have closely similar frequencies and are completely defined by the longitudinal vibrations of the terrace atoms.

The modes that propagate along the $\overline{\Gamma}\,\overline{Y}$ direction (normal to the step) are reflected modes that are inherent in the given direction of the simple (111) surface.[59] The reflection appears due to the change of the unit cell dimensions caused by the decrease in the surface symmetry.

Table 4. Energies of phonon modes at the symmetrical $\overline{\Gamma}$, $\overline{X}$ and $\overline{Y}$ points of relaxed Cu(211) film.

BZ point	Mode	Our EAM calculation [47]	EAM [5, 60]	*Ab initio* calculation [62]	HAS [108]
$\overline{\Gamma}$	X_1X_3	9.5	–	–	–
	Z_2Z_3	10.8	9.8	11.5	10.9 ± 0.2
	Y_2	23.6	25.9	24.7	–
$\overline{X}$	$E_1(YZ)_{13}$	10.3	11.3	–	11.7
	$(ZY)_2$	12.0	–	–	13.3
	$E_2(ZY)_1$	13.3	14.0	–	14 ± 0.1
	$ME_3(X)_{13}$	26.1	–	–	26.6
$\overline{Y}$	$(X)_{12}$	4.9	–	–	–
	$(ZY)_1, (Z)_{34}$	6.2	6.2	–	5.5 ± 0.2
	Z_3	6.6	6.7	–	7.6 ± 0.4
	$(YZ)_{12}$	11.6	11.7	–	10.5 ± 0.3

Note. The polarization atomic displacements X, Y, Z coincide with the $[0\bar{1}1]$, $[\bar{1}11]$ and $[\bar{2}11]$ directions, respectively.

For the Cu(211) surface, both experimental [108, 160] and theoretical [47, 60] data are available, including *ab initio* calculation data [62] for the energy of phonon modes in symmetrical points of the BZ, which are presented in Table 4. It can be seen that EAM calculation reproduces the phonon spectrum of the Cu(211) surface with good accuracy. Analysis of the phonon spectra of the (211) vicinal surfaces of other FCC metals (Al, Ni, Ag, Pd) demonstrated their full qualitative similarity with the phonon spectrum of the Cu(211) surface.[47, 60, 62] The differences are only in the energies of the vibrational modes and localization degrees of these modes on surface layers.

b. Phonon spectra of class *B* vicinal surfaces

The (311) and (511) surfaces refer to class *B* (see Table 2) and are formed by terraces in the (100) plane and steps with (111) orientation. The unit cell of the (311) surface comprises two atoms (a terrace atom and a step-edge atom), and that of the (511) surface contains three atoms (two terrace atoms and a step-atom). The dispersion curves for these copper surfaces are shown in Fig. 7. The calculation was performed for ideal and relaxed films, a 45-layer film for Cu(311) and a 81-layer film for Cu(511). In both cases, the phonon spectra exhibit step modes. However, whereas the (311) surface has the transverse modes E_1 and E_2, in the (511) surface, shear modes with vertical (SV) or horizontal (SH) polarization predominate. The relaxation of the (311) surface increases the step mode energy: at the BZ boundary, along the $\overline{X}\,\overline{S}$ direction, they shift towards the bulk vibrational region and partially lose their surface nature. Owing to relaxation, an additional surface state with the longitudinal polarization appears in the forbidden gap.

For the vicinal (511) surface, relaxation brings about modification of the phonon spectrum in the vicinity of the forbidden gap. The energy of the surface state localized on the third layer of an ideal surface increases; while being displaced to the region of bulk vibrations, this state becomes a resonance. As in the case of the (311) surface, a new longitudinal surface state localized on the step atoms and the corner atom of the terrace appears in the forbidden

gap. A typical feature of the phonon spectrum of the (511) surface is the presence of longitudinal resonance localized on the step along the $\overline{\Gamma}\,\overline{X}$ direction. First, it is manifested as a surface mode with simultaneous localization of the vibrational state (~80%) on step and terrace atoms. However, when $\mathbf{q}_x \approx 0.25|\overline{\Gamma}\,\overline{X}|$, it transforms into a longitudinal resonance localized only on the step and reaching the BZ centre.

Experimental[108, 160, 166] and theoretical[47, 60–62] studies of the surface phonon dispersion were carried out for Cu(511). While comparing the energies of surface modes presented in Table 5, one can see good agreement. The experimental value of the SV mode at the $\overline{X}$ point is somewhat higher than the calculated value, which may be associated with the difficulty of experimental determination of the energy of this mode. There is some uncertainty caused by low intensity of the recorded vibrational peaks near the zone boundary.[108]

Table 5. Energies of phonon modes at the symmetrical $\overline{\Gamma}$, $\overline{X}$ and $\overline{Y}$ points of the relaxed Cu(511) surface.

BZ point	Mode	Our EAM calculation [47]	EAM (see [5, 60])	HAS [108] (LEES [166])
$\overline{\Gamma}$	X_1X_3	7.0	–	11.3
	Z_{12}	10.8	11.7	11.5 ± 0.2
$\overline{X}$	SH	9.9	11.4	11.2
	SV	12.9	13.4	13.5 ± 1
	$(YZ)_{13}$	14.3	14.5	16.0 ± 1
	$Z_1, (YZ)_2$	25.6	25.5	25.5–26.6
$\overline{Y}$	$(X)_{13}$	4.6	5.8	5.8
	$(YZ)_{13}$	6.6	6.5	6.3 ± 0.3
	$(YZ)_{12}$	11.8	13.4	14.4

Note. The polarization atomic displacements X, Y, Z coincide with the $[0\bar{1}1]$, $[\bar{2}55]$ and [511] directions, respectively.

Rahman *et al.*[5] analyzed the change in the force constants on the Cu(511) surface. It was shown that the force constant F_{xx} in the plane between atoms located along the step in the direction normal to the step is attenuated (softened) by 93% compared with its analogue in the bulk. The softening is caused by a decrease in the number of neighbours and results in the decrease in the frequency of the longitudinal mode propagating along the direction y (normal to the step). The force constant F_{zz} between the step atoms and their close neighbours in the bulk is enhanced by 35%, which is a consequence of the bond shortening by 2.3%. Similar results were obtained for the (211) and (331) surfaces: F_{xx} decreases by 86% and 85%, and F_{zz} increases by 30% and 45%, respectively. Unlike simple surfaces, the off-diagonal elements of the force constant matrix also change. For example, F_{xz} and F_{yz} for the (511) surface increase by 30% and 35%, respectively. This change in the force constants was also found for Ni(977), Au(511) and Al(511).[61, 167] It is evident that similar trends are also inherent in other transition metals. The phonon spectra of the (511) surfaces of other FCC metals (Ni, Ag and Pd) are qualitatively similar and differ only by the energies of the principal modes.

c. Phonon spectra of class *C* vicinal surfaces

The class *C* vicinal surfaces, (331) and (221), are formed by a terrace and a step, which have the same (111) orientation. The phonon spectra of the relaxed Cu(331) and Cu(221) surfaces are shown in Fig. 8. The unit cell of the (331) surface contains three atoms as in the case of the (211) surface, *i.e.*, geometrically these surfaces are similar. In the phonon spectrum of Cu(331), as in the spectrum of Cu(211), three step-localized surface states were detected — E_1, E_2 and ME_3 (see Fig. 8 *a*). The main distinction from the (211) surface is in the fact that the mode E_1 lies much closer to the surface states localized on terrace atoms and exists as the step mode only in the range from point $\overline{X}$ to $\mathbf{q}_x \approx 0.8|\overline{\Gamma}\,\overline{X}|$. Then it transforms into a resonance mode having polarization similar to that of the Rayleigh mode of the (111) surface. This behaviour of the step mode does not contradict the data of Knipp;[59] the energies of the mode E_1 at the $\overline{X}$ point also agree: 11.99 and 12.06 meV, respectively.

Upon decrease in the wave vector (from point $\overline{X}$ to point $\overline{\Gamma}$), the second step mode E_2 caused by SH displacements of atoms is mixed with the bulk states and transforms into a resonance. Note that unlike the (211) surface, in this case, the type of atomic displacements relative to the normal to the surface changes. Whereas in the (211) surface, the step mode E_1 is mainly caused by SH vibrations and the step mode E_2 is caused by SV vibrations, in the (331) surface they change the type of vibrations to the opposite one. One more difference is that the step mode ME_3 in the (331) surface has a weak localization being highly coupled with bulk vibrations. Such a character of vibrations and their lower degree of localization on the step are consequences of the abnormal type of relaxation of the given surface. Since the corner atom shifts towards the bulk (the corner atoms of all other surfaces tend to shift upon relaxation away from the bulk), this shortens the bond to the nearest bulk atom located below the step and corresponding to the increase in the force constants.[5]

At the $\overline{\Gamma}$ point, there is a high-frequency state — a reflected surface mode located in the forbidden gap of the (111) surface and corresponding to the SH displacements of the terrace atoms. The Rayleigh mode is formed by coupled vibrations of the terrace and step atoms in the sagittal plane and is manifested in the vibration spectrum only as a reflected mode in the $\overline{\Gamma}\,\overline{Y}$ direction.

On going from the (331) to (221) surface, the number of atoms in the unit cell increases to four and one should expect complication of the phonon spectrum of this surface. For the Cu(221) surface (see Fig. 8 *b*), it is usual that at the $\overline{X}$ point, there is a group of surface states located below the boundary of bulk vibrations and having very similar energy values differing by only ~0.5 meV. The lower state is a typical step mode E_1 mainly with SV displacements of atoms. This is followed by the Rayleigh mode localized on the terrace (~60%), which is due to the vibrations of the second- and third-layer atoms. In the case of the ideal, non-relaxed (221) surface, the step mode E_2 is located below the bottom of the projection of bulk states and has a clear-cut surface character. As a result of relaxation displacements of atoms, it gets into the region of bulk vibrations and becomes a resonance along the whole $\overline{X}\,\overline{S}$ direction. At the $\overline{Y}$ point and along the $\overline{\Gamma}\,\overline{Y}$ direction, the lower mode is associated with longitudinal displacements along the step. Other states in this direction are the reflected modes of the (111) surface that propagate in the sagittal plane. At the $\overline{\Gamma}$

point, there are two resonance states localized mainly on the step. Each comprises two virtually degenerate states with energies differing by $\sim$0.4 meV. The low-frequency state is characterized by transverse displacements of atoms in the sagittal plane and has an energy of 10.34 meV, which is consistent with the experimental[167] value of the energy of this mode (10.95 meV).

For the (221) surface, experimental data are available only for aluminium. Using the HAS the method,[160] a resonance step mode with SV polarization was detected in the vicinity of the $\overline{\Gamma}$ point. The step mode propagates along the $\overline{\Gamma}\,\overline{X}$ direction without any dispersion to $\mathbf{q}_x \approx 0.4|\overline{\Gamma}\,\overline{X}|$, which is consistent with the behaviour of the lower of the two step modes obtained by EAM calculation for the $\overline{\Gamma}$ point. The same step mode is also found in the $\overline{\Gamma}\,\overline{Y}$ direction at low values of the wave vector. At the $\overline{\Gamma}$ point at the energy of 10.95 meV and along the $\overline{\Gamma}\,\overline{Y}$ and $\overline{\Gamma}\,\overline{X}$ directions, a mode whose polarization remained not entirely clear was found experimentally. According to EAM calculation, at low $\mathbf{q}_x$ values, this mode has an SH polarization, its energy (11.34 meV) being in line with the experimental value (10.95 meV). The phonon spectra for the (331) and (221) surfaces of other FCC metals are qualitatively similar and differ only by the energy of vibrational modes.

Analysis of the phonon spectra of the considered Al, Cu, Ag, Ni and Pd vicinal surfaces demonstrated that they have common features determined only by the structural type of the metal and do not depend on its chemical nature. The vibrational spectra of the vicinal surfaces of FCC metals display the dipole-active resonance at the centre of the Brillouin zone; this resonance is determined by strictly *z*-polarized coupled vibrations of step atoms and the nearest terrace corner atom. In all vicinal surfaces of FCC metals, coupled vibrations of a new type localized on the step appear. Depending on the structural type of the surface, the step phonon is associated with atomic vibrations perpendicular to the step (mainly in the surface plane) or along the normal to the surface. In the phonon spectra of vicinal surfaces at the centre of BZ (point $\overline{\Gamma}$), there is a pseudogap, which appears upon reflection of the phonon modes of the simple surface whose fragment is the terrace. In this pseudogap, a longitudinal resonance localized on the step and propagating deep into the bulk is always present. The nature of the metal affects the energies of the phonon modes and degrees of their localization on the step or terrace atoms. The structural relaxation is critical for the vibrational modes located on or near the step, because this leads to a change in their localization on the step atoms. Comparison of the results of EAM calculation of the energies of principal step modes with the experimental results and data from other calculations showed a good agreement. This validates the use of EAM for description of phonons on surfaces having step defects.

3. Phonons in adsorption structures

It was shown both theoretically and experimentally[52–56,63,69,89,168–199] that at low coverages ($\leqslant$1 monolayers), the phonon subsystem of the adsorption structure is determined by two principal modes localized on adatoms. One of these, the stretching S mode, is polarized strictly perpendicular to the surface and is due to coupled vibrations of the adatom and the nearest substrate atoms. The second one, the longitudinal mode of frustrated translations (FT mode) has a reciprocating translation nature due to the interaction with vertical vibrations excited in the surface layer of the substrate. It was shown[54,69] that the energy of the S mode for coverages $\theta \geqslant 0.25$ monolayers (ratio of the number of adatoms to the number of surface atoms contained in the unit cell) almost does not depend on the coverage up to a saturated monolayer state but the mode localization on adatoms decreases. The FT mode, conversely, is highly dependent on the coverage, the energy of the FT mode being increased as the coverage increases.

Both modes are sensitive to the adsorption geometry and the substrate structure.[53,55] By investigating the variation of the energy of these modes, it is possible to gain information about the dynamically stable adsorption geometry for different sites and degrees of adsorption on the substrate surfaces with different crystallographic orientations. However, until recently these aspects of the dynamics of adsorption structures have not been studied. Only two papers[69,168] report analysis of the dependences of the S mode energy on the adsorbate mass and demonstrated that the energy depends linearly on a quantity equal to the reciprocal square root of the adsorbate mass. However, since this conclusion was based on scanty experimental data obtained for surfaces with different orientations and coverages and for different substrate materials, and mainly for the BZ centre, this complicates elucidation of the general trends of formation of dynamically stable adsorption structures. It is evident that analysis of the effect of various factors on the behaviour of the principal vibrational modes requires that the vibrational structure of the adsorbates be considered under equal conditions, in particular, adsorption geometry, coverage and orientation and chemical type of the substrate. Important also is the description of the dispersion curves along all symmetrical directions of two-dimensional BZ of the adsorbate and the substrate.

Data on the investigation of the vibrational characteristics of alkali metal/metal adsorption systems are summarized in Table 6. It can be seen that experimenters pay quite a lot of attention to this issue. The most comprehensive theoretical study of the dependence of vibrational properties of adsorption structures on the adsorption geometry and coverage and the substrate material and orientation was carried out using EAM potentials.[52–56] Below we summarize the experimental and theoretical studies on the dependence of the principal vibrational modes of the adsorbate on the above-indicated factors. All theoretical calculations were carried out using the EAM potentials.

The Al(111)$-(\sqrt{3}\times\sqrt{3})$R30°$-$(Li, Na, K) systems are very convenient for the study of the effect of the atom masses and adsorption geometry on the phonon spectrum as the atomic masses of lithium, sodium and potassium are considerably different, while the chemical type of the adsorbate remains the same. It is known that at room temperature, alkali metal atoms are adsorbed according to the substitutional mechanism into six-fold sites.[69] As this takes place, they form a surface alloy with the substrate atoms[72,83–86,169–180] with a period of $(\sqrt{3}\times\sqrt{3})$R30°. This is due to the fact that thermally activated vacancies appear on the surface of the aluminium substrate; adatoms occupy these vacancies and form a substitutional superstructure. A similar structure but consisting only of adatoms is formed when the atoms are adsorbed at three-fold sites at low temperature. If the substrate is then slowly heated to room temperature, transition to the substitutional structure takes place. This transition is irreversible and the structure

Table 6. Experimental and theoretical data on the phonons in the adsorption superstructures.

System	Structure		Phonons			
	θ /monolayer	periodicity	experiment	Ref.	calculation	Ref.
Li/Al(100)	0.5	c(2 × 2)	–	–	EAM	55
Na/Al(100)	0.5	c(2 × 2)	–	–	EAM	55
Li/Al(111)	0.33	$(\sqrt{3}\times\sqrt{3})$R30°	HREELS	85	EAM	53
Na/Al(111)	0.33	$(\sqrt{3}\times\sqrt{3})$R30°	HREELS, HAS	85, 69	EAM, DFT, FC	53, 83, 169
K/Al(111)	0.33	$(\sqrt{3}\times\sqrt{3})$R30°	HAS	69	EAM	53
Cs/Al(111)	0.33	$(\sqrt{3}\times\sqrt{3})$R30°	HAS	69	DFT	83
Li/Cu(111)	0.11	p(3 × 3)	HREELS	183	–	–
Na/Cu(111)	0.25	p(2 × 2)	HREELS	184	EAM, DFT, jelly model	56, 76, 190
K/Cu(111)	0.33	$(\sqrt{3}\times\sqrt{3})$R30°	HREELS	184, 198	–	–
Cs/Cu(111)	0.44	(3/2 × 3/2)	HAS	193	–	–
Li/Cu(100)	0.02–0.5	c(2 × 2)	HREELS	199	EAM	56, 134
Na/Cu(100)	0.02–0.5	c(2 × 2)	HREELS, HAS	63, 192, 198	EAM, FC	56, 64, 134
K/Cu(100)	0.02–0.5	c(2 × 2)	HRLEES, HAS	64, 198	–	–
Cs/Cu(100)	0.02–0.5	c(2 × 2)	HAS	191	–	–
Li/Cu(110)	0.14	(1 × 2)	HREELS	199	EAM	134
Na/Cu(110)	0.31	(1 × 3)	HREELS	198, 199	EAM	134
K/Cu(110)	0.31	(1 × 3)	HREELS	198, 199	–	–
K/Ni(100)	2–5	(1 × 3)	HAS	193	–	–
K/Ni(110)	0.26–0.48	c(2 × 2)LT-Ni(1 × 1) (1 × 2)RT-Ni(1 × 2)	HREELS	194	–	–
Na/Pt(111)	0.22–0.41	(2 × 2)	HAS	193	–	–
K/Pt(111)	0.22–0.41	$(\sqrt{3}\times\sqrt{3})$R30°	HREELS	195, 196	EAM, DFT	57, 195
			TRSHG	186	–	–
Cs/Pt(111)	0.22–0.41	$(\sqrt{3}\times\sqrt{3})$R30°	TRSHG	197	–	–

Note. The following designations are used: LT is low temperature, RT is room temperature, TRSHG is time-resolved second harmonics generation, FC is the force constant model.

formed at low temperature is metastable.[171] For the Al(111)–$(\sqrt{3}\times\sqrt{3})$R30°– (Li, Na, K) systems, the energies of vibrational modes have been determined experimentally (see references in Table 6), which can be used to verify the adequacy of EAM calculations.

a. Effect of the atom size and adatom mass on the phonon spectrum

Experimental HREELS studies of the phonon spectrum of the Al(111)–$(\sqrt{3}\times\sqrt{3})$R30°–Na system were carried out by Nagao *et al.*[85, 169] The dispersion curves along the $\overline{\Gamma}\,\overline{K}'$ direction of a planar BZ were studied in detail and two resonance acoustic modes, R1 and R2, were described: both modes are localized on adatoms and are polarized perendicular to the surface. The mode R1 is found at the $\overline{\Gamma}$ point at an energy of 12.5 ± 0.2 meV, while the mode R2 demonstrates a strong dispersion dependence and propagates deep in the bulk in the $\overline{\Gamma}\,\overline{K}'$ direction. At the BZ boundary (point $\overline{K}'$), in the gap between the bulk band and the lowest surface mode, the vibrational mode S1 occurs in the energy range of 10.8–11.5 meV.[177] Using the HAS method, a similar S1 mode with the energy of 9.2 meV was found[69] at the $\overline{K}'$ point. A DFT calculation gives the 12.8 meV energy for the mode R1.[83] For the Al(111)–$(\sqrt{3}\times\sqrt{3})$R30°–Li system, experimental values of the energy of the mode R1 at the $\overline{\Gamma}$ point have also been obtained (17.6–18.1 meV).[177] Nagao *et al.*[169] studied the dispersion of phonons along the $\overline{\Gamma}\,\overline{K}'$ and $\overline{\Gamma}\,\overline{M}$ directions in the Al(111)–$(\sqrt{3}\times\sqrt{3})$R30°–K structure. A state was found that corresponds to the Rayleigh mode of the clean surface but is shifted by 1–2 meV to higher frequencies. The surface mode R1 was found at the $\overline{\Gamma}$ point at 6.4 meV. The *ab initio* calculation for the non-relaxed Al(111)–$(\sqrt{3}\times\sqrt{3})$R30°–K structure afforded the value of energy for this mode to be 8.2 meV.[83]

The model of adsorption structure $(\sqrt{3}\times\sqrt{3})$R30° with adatoms in three- and six-fold sites and the corresponding two-dimensional BZ are shown in Fig. 9. Since the BZ of the $(\sqrt{3}\times\sqrt{3})$R30° unit cell is three times smaller than the BZ of the ideal (1 × 1) cell, it reflects the symmetrical points of the BZ of the ideal unit cell (see Fig. 9 *c*). The reflection occurs according to the following principle:

$$(\sqrt{3}\times\sqrt{3})\text{R30}^\circ \longrightarrow (1\times1) \longrightarrow$$
$$\longrightarrow (\overline{\Gamma}\leftarrow\overline{K},\overline{\Gamma});(\overline{K}'\leftarrow 2/3\,\overline{\Gamma}\,\overline{M});(\overline{M}'\leftarrow 0.5\,\overline{\Gamma}\,\overline{K},\overline{M})$$

When sodium adatoms are in six-fold sites, they displace every third atom of the substrate and form an ordered surface alloy with the periodicity of $(\sqrt{3}\times\sqrt{3})$R30° (adatoms and atoms of the substrate surface layer are nearly in one plane). The equilibrium bond length (between the sodium adatom and the nearest aluminium atom) calculated using the EAM potentials is $d_{\mathrm{Na-Al}} = 3.22$ Å. This value is in good agreement with the experimental values, 3.31 ± 0.03, 3.10 ± 0.06, 3.21 and 3.21 ± 0.01 Å, obtained in a number of publications.[172–174, 181] The adsorption induces relaxation effects in the substrate: the first interlayer spacings decrease by $\Delta_{12} = -5.4\%$ and $\Delta_{23} = -0.15\%$, which is in qualitative agreement with

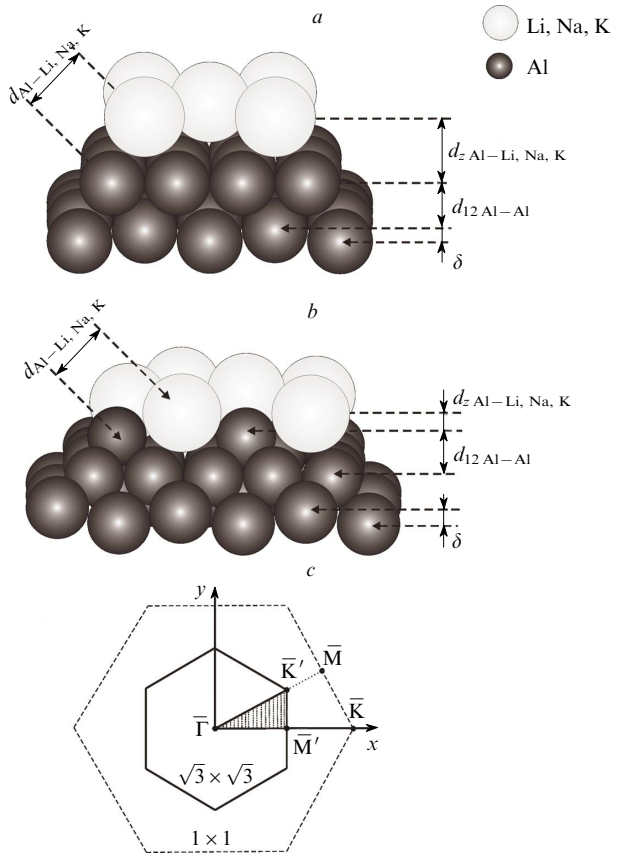


Figure 9. Geometric model of the $(\sqrt{3}\times\sqrt{3})R30^\circ$ adsorption structure (*a*, *b*) and the corresponding two-dimensional BZ (shaded area) in comparison with the BZ of the (1×1) unit cell (*c*).[53]
(*a*) Adatom adsorption; (*b*) substitutional adsorption; d_z is the distance from the adatom to the substrate, $d_{Al-Li,\ Na,\ K}$ is the bond length, $d_{12\ Al-Al}$ is the first interlayer spacing in the substrate, δ is the rippling parameter of the subsurface layer of the substrate.

LEED data[81] ($\Delta_{12} = -3\%$) and *ab initio* calculation ($\Delta_{12} = -2.5\%$).[83] The subsurface layer is rippled (the atoms located directly below the adatom shift toward this atom by larger distances than other atoms). The calculated rippling value is $\delta = 0.0017$ Å, which is comparable with the experimental result $\delta = 0.0015$ Å.[174] Analysis of the interatomic interactions demonstrated that the force constants between the closest atoms of the first and second layers of the substrate increase by 16%–19% with respect to the values for clean surface. The *z*-component of the force constants of the surface layer change insignificantly, whereas for the second and third layers it increases by 9%. In these layers, the tangential components of the force constants are also markedly enhanced.

The phonon spectrum of the Al(111)–$(\sqrt{3}\times\sqrt{3})R30^\circ$–Na system (substitutional adsorption) simulated using the EAM potentials is shown in Fig. 10. Apart from the reflected states related to the substrate vibrations, point $\overline{\Gamma}$ has a *z*-polarized resonance mode R1, which can be considered as reflection of the mode R2 related to the new periodicity $(\sqrt{3}\times\sqrt{3})R30^\circ$. The calculated energy of the mode R1 (12.76 meV) is in good agreement with the experimental value (12.5 meV).[169]

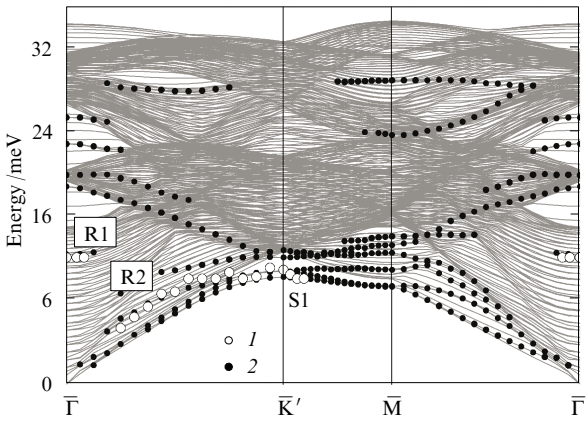


Figure 10. Phonon spectrum of the Al(111)–$(\sqrt{3}\times\sqrt{3})R30^\circ$–Na system (substitutional adsorption).
(*1*) Experiment,[169] (*2*) calculation.[53]

Investigation of the character of localization and polarization of this mode showed that this is a coupled surface resonance with vertical displacements of adatoms and the substrate surface atoms. The upper state at the $\overline{\Gamma}$ point (23.74 meV) is localized on the sodium and aluminium atoms in the surface alloys and involves atomic displacements in the surface plane. The other modes at the centre of BZ are typical of a clean Al(111) surface but now they are caused by cooperative displacements of sodium and aluminium atoms.

Along the $\overline{K}'\overline{M}$ direction at large values of the wave vector **q**, there are surface modes located below the bottom of the projection of bulk phonons. One of these (along the $\overline{\Gamma}\,\overline{M}$ direction) is coupled with longitudinal vibrations of the first-layer substrate atoms, while the other is similar to the Rayleigh mode of the substrate. When the **q** values are small they are mixed with bulk phonons and become resonances. At the $\overline{K}'$ point, the energies of these modes are 10.6 and 11.2 meV, respectively, which is in line with experimental data.[169, 176] The calculated energy of the mode S1 (9.6 meV) at the $\overline{M}$ point is also in good agreement with the experimental value (9.2 meV).[176] Polarization and localization analysis demonstrated that S1 is the coupled mode caused by vibrations of adatoms and substrate surface layer atoms in the sagittal plane. This type of vibrations in the sagittal plane is inherent in the Rayleigh mode of the substrate.

The other experimentally[176] determined mode (R2) is a transverse resonance propagating along the $\overline{\Gamma}\,\overline{K}'$ direction. As regards the character of vibrations, it also resembles the Rayleigh mode of the substrate but, unlike S1, it is located above the boundary of the bulk phonon region. Some authors[69, 160] detected a similar mode by means of HAS but at 1–2 meV higher energy compared with the energy of the clean-Al(111) Rayleigh mode.[182] This behaviour is related to the normal (*z*) component of force constants between the neighbouring aluminium and sodium atoms. In the presence of a superstructure induced by the adsorbate, the normal component of force constants is non-zero (unlike the clean aluminium surface). Sodium adatoms are not completely embedded into the upper layer of the substrate, being partially located above the surface; there-

fore, normal interactions appear and the mode R2 shifts to the region of bulk vibrations. It should also be noted that the modes of the clean Al(111) surface are reproduced in the phonon spectrum along all directions of the BZ; however, in the case considered, they are degenerate with the adsorbate phonons and are coupled. The presence of the adsorbate induces also their frequency shift but does not affect polarization.

Due to their small size, the lithium atoms penetrate into the surface layer of the aluminium substrate much deeper than sodium atoms. After relaxation of the Al(111)–($\sqrt{3}\times\sqrt{3}$)R30°–Li system, the calculated bond length between the lithium atom and the nearest substrate atom is 3.10 Å and the experimental value determined by Nielsen *et al.*[177] is 2.88 Å. The first interlayer spacing in the substrate is shortened ($\Delta_{12} = -5.1\%$), which is also qualitatively consistent with experimental data ($-2.1 \pm 1\%$).[177] As in the case of sodium adsorption, a minor ($\delta = 0.0016$ Å) rippling of the structure in the subsurface layer of the substrate occurs. The interlayer spacings for deeper layers correspond to the bulk values.

The *z*-polarized surface resonance localized on adatoms was detected at the $\overline{\Gamma}$ point at 21.3 meV energy. The same resonance was found experimentally[85] at an energy of ~17.6–18.1 meV. As in the case of sodium adsorption, there are surface modes along the $\overline{K}'\overline{M}$ direction, below the bottom of the projection of bulk phonons. However, they are localized only on substrate atoms. The modes related to the vibrations of lithium adatoms are shifted to higher energies and propagate deep into the bulk phonon region. Force constant analysis showed enhancement of the interaction between the lithium adatoms with atoms of the subsurface layers of the substrate. The Li–Al_3 interaction (third layer) increases by 27% compared to interlayer Al_1–Al_3 interaction of the clean surface.

Potassium atoms are larger than lithium or sodium atoms; therefore, potassium cannot be embedded into the substrate to a considerable depth; it is actually located

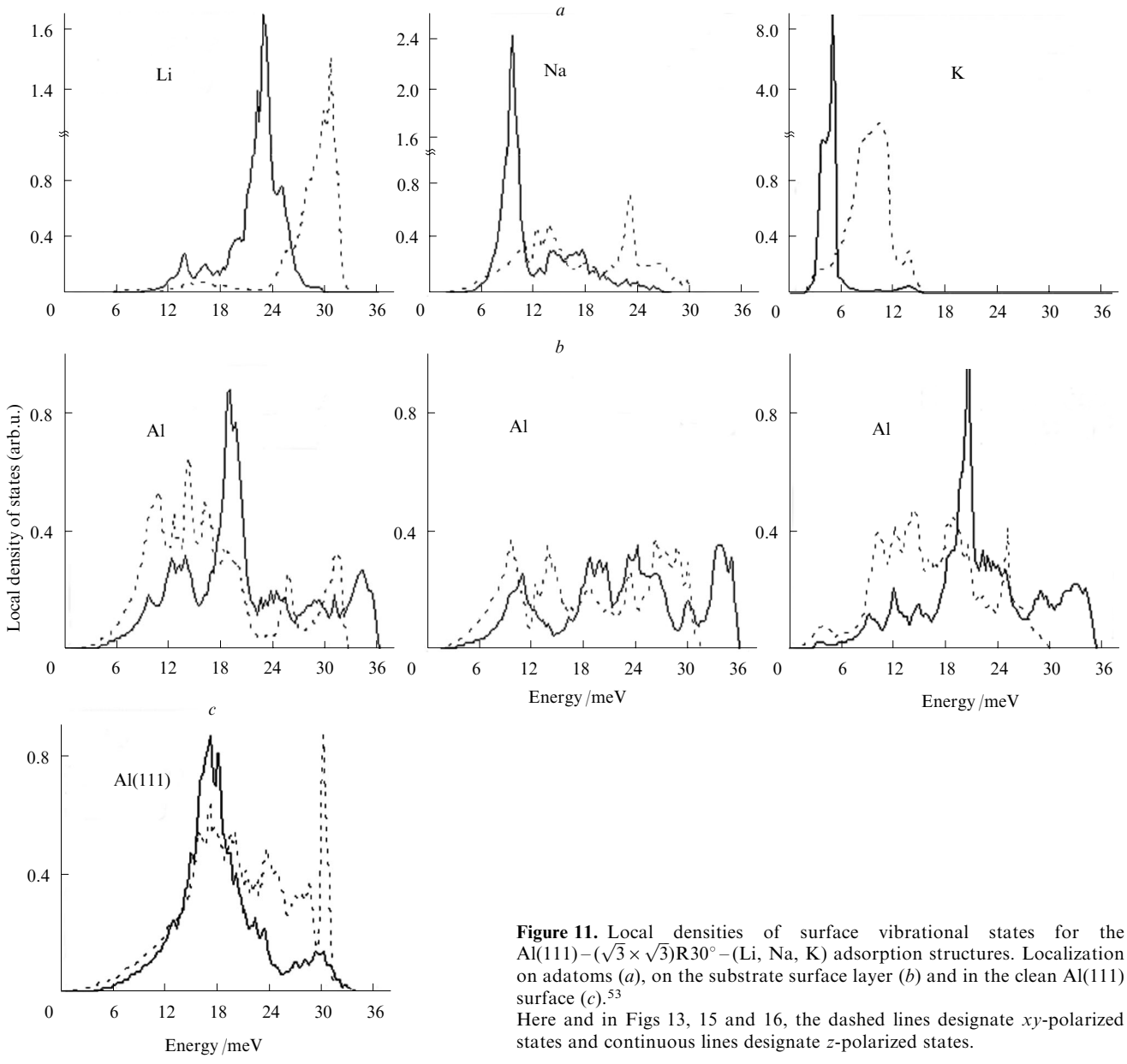


Figure 11. Local densities of surface vibrational states for the Al(111)–($\sqrt{3}\times\sqrt{3}$)R30°–(Li, Na, K) adsorption structures. Localization on adatoms (*a*), on the substrate surface layer (*b*) and in the clean Al(111) surface (*c*).[53]
Here and in Figs 13, 15 and 16, the dashed lines designate *xy*-polarized states and continuous lines designate *z*-polarized states.

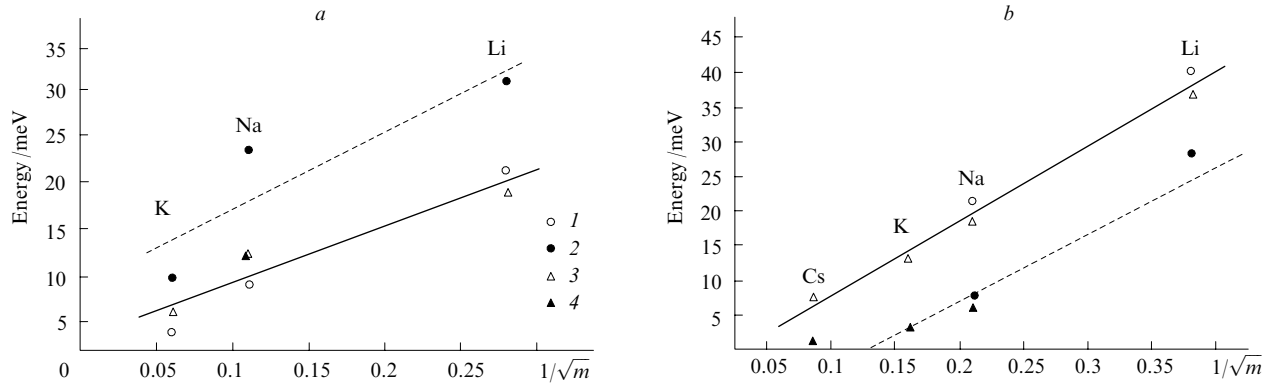


Figure 12. Vibrational energy *vs.* adatom atomic radius and mass for substitutional adsorption for the alkali metal/Al(111) system (*a*) and for adatom type-adsorption for the alkali metal/Cu(100) system (*b*).
The continuous and dashed lines designate vertical and longitudinal vibrations, respectively.
(*1*) EAM calculation, vertical vibrations; (*2*) EAM calculation, longitudinal vibrations; (*3*) experiment, vertical vibrations; (*4*) DFT calculation, vertical vibration (*a*) and experiment, longitudinal vibrations (*b*). The results were taken from experimental works,[63, 69, 85, 191, 198, 199] the DFT data are from Ref. 83 and EAM data are from Refs 53, 56, 134.

above the six-fold vacancies of the substrate. For the surface structure Al(111)–$(\sqrt{3}\times\sqrt{3})$R30°–K, the equilibrium bond length $d_{\mathrm{Al-K}}$ after the relaxation was 3.67 Å (for comparison, $d_{\mathrm{Li-Al}}$ = 3.10 Å, $d_{\mathrm{Na-Al}}$ = 3.22 Å). This EAM value is consistent with experimental results (LEED)[175, 176] and *ab initio* calculations (DFT),[83] which are 3.58 and 3.70 Å, respectively. Due to this position of adatoms, the K–Al interaction along the normal to the surface becomes weaker but simultaneously the interaction of adatoms with one another becomes stronger. Examination of the force constants demonstrated that the Al–K interaction is 4.5 times weaker than the Al–Al interaction in the surface layer of the substrate. This behaviour of force constants is related to the fact that for potassium adsorption, shielding is weak, which was estimated during the calculation of the electronic structure.[71] The presence of potassium adatoms also leads to relaxation of the surface layers (Δ_{12} = −4.15%, Δ_{23} = −0.13%); however, unlike adsorption of sodium and lithium, no rippling of the structure was noted for subsurface layers

A state corresponding to the Rayleigh mode of the clean surface was found in the phonon spectrum along the $\bar{\Gamma}\bar{K}'$ and $\bar{\Gamma}\bar{M}$ directions. A similar mode was detected in the HAS experiment.[69] At the $\bar{\Gamma}$ point, the *Z* mode (4.22 meV) mainly localized on the potassium adatom corresponds to the *z*-polarized mode experimentally [69] detected at 6.4 meV. It propagates along all symmetrical BZ directions without changing its energy. Apart from the direct calculation, the energy of this mode was estimated from force constant and adatom mass analysis.[53, 134] The normal component of the force constant between potassium and the nearest substrate atom is ~5.3 times lower than in the case of the sodium adatom and the potassium atomic mass is 1.7 times greater than the sodium atomic mass. Thus, the frequency of *z*-polarized vibrations of the potassium adatom on the Al(111) surface should be ~3 times lower than the frequency of the corresponding sodium mode, which was actually confirmed in our EAM calculation.[53] The group of states located below the bottom of the projection of bulk phonons corresponds to longitudinal vibrations of potassium and surface aluminium atoms. The decrease in energy of longitudinal vibrations of the substrate atoms (compared with the energy of similar vibrations in the case of sodium or lithium adsorption) is related to the decrease in the intralayer Al–Al force constants by 12%, whereas in the case of sodium and lithium adsorption, they almost do not change with respect to the force constants for the clean aluminium surface. As in the case of sodium adsorption, *x*- and *y*-polarized potassium modes are split, which is related to the substrate surface geometry (non-uniform atomic environment along the $[1\bar{1}0]$ and $[11\bar{2}]$ directions). Note the key distinction of the vibrational spectrum for the K/Al(111) system: all of the adatom-localized modes, except for the $\bar{\Gamma}$ point, are located below the bottom of the bulk phonon region.

The effect of adsorbate type is manifested most clearly in the distribution of the local density of vibrational states presented in Fig. 11. It can be seen by the arrangement of localized peaks that the excitation energy of the transverse S mode, which represents coupled vibrations of adatoms and substrate atoms, is lower than the energy of the mode of coupled translational displacements of adsorbate atoms. This energy ratio of the adsorbate vibrational modes reflects the dominance of the adatom–substrate bonding. Also, one can follow the dependence of the energy of the principal vibrational modes of the adsorbate on the adatom atomic radius and mass (see Figs 11 and 12).

The effect of adatoms on the phonon structure of the substrate can be followed by comparison with the local density of vibrational states of clean Al(111) surface (see Fig. 11 *c*). This effect is manifested only for the first two atomic layers as softening of all longitudinal modes of the substrate. The Rayleigh mode of the substrate is most affected by sodium adatoms: it completely smears, localization reduces more than twofold and high-frequency shift occurs. The potassium and lithium adatoms induce minor changes in the vibrational spectrum of the substrate, mainly increasing the energy of the Rayleigh mode. It is noteworthy that despite the change in energy and localization degree, all modes of the substrate retain their polarization. Also, new vibrational states appear that are initiated by the presence of adatoms and are not typical of a clean Al(111) surface.

b. Effect of the adsorption geometry on the phonon spectrum

Effect of the adsorption geometry on the vibrational properties were studied in relation to the Al(111)–$(\sqrt{3}\times\sqrt{3})$R30°–Na system. As described above, at low temperature ($T \leqslant 100$ K), the sodium atoms being adsorbed in three-fold sites, form an adatom-type superstructure on the Al(111) surface with the periodicity of $(\sqrt{3}\times\sqrt{3})$R30°, as also in the case of high-temperature substitutional adsorption [180] (see Fig. 10). The equilibrium adatom–substrate distance (h_{Na-Al}) for this geometry was 2.72 Å, which is almost twice greater than in the case of substitutional adsorption (1.4 Å). Force constant analysis demonstrated weakening of the adatom–substrate interactions.

In the phonon spectrum of the Na/Al(111) system, a very soft, a low-frequency longitudinal mode appears due to the coupled translational displacements of adatoms parallel to the substrate surface. Note that the longitudinal mode energy equal to 3.4 meV remains invariable along all BZ directions. Upon elastic interaction with the substrate, it excites low-frequency transverse vibrations of the surface layer atoms in the substrate. About 93% of localization of the vibrations is on adatoms and only 7% is on the first-layer atoms of the substrate, which are displaced in the sagittal plane. Actually this is the mode of translation of adsorbate atoms weakly connected to the substrate. Although this vibrational state is manifested along all symmetrical directions of the two-dimensional BZ, its experimental detection is difficult, because it propagates strictly parallel to the surface.[69, 169]

A low-frequency longitudinal mode highly localized on the subsurface layer atoms of the substrate appears in the phonon spectrum of the substrate in the vicinity of the $\overline{\Gamma}$ point. The presence of this mode is not inherent in a clean surface; it appears due to interaction of a sodium adatom with the second-layer atoms of the substrate located directly below it. At the $\overline{K}'$ point, a *z*-polarized mode with the energy of 11.25 meV was detected experimentally; it was assumed that this mode is completely localized on the

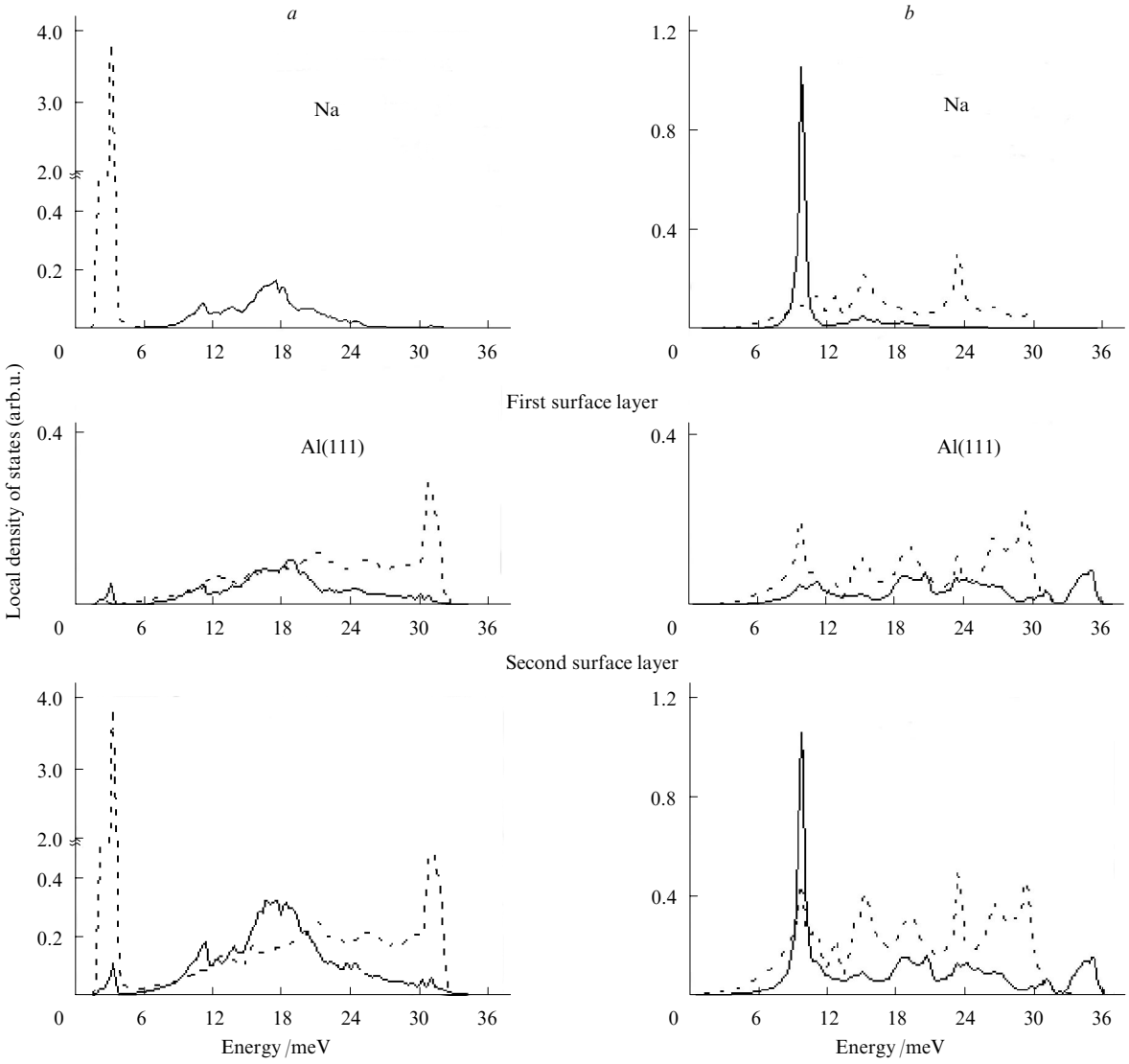


Figure 13. Local densities of vibrational states upon sodium adsorption on the Al(111) surface in three-fold (*a*) and six-fold (*b*) adsorption sites.[52, 54]

sodium adatoms.[69] EAM calculation showed [57] the presence of this mode at the $\overline{K}'$ point at 11.4 meV but it was found to be localized on adatoms (~30%) and on the first-layer substrate atoms (~42%).

The state density distributions for both adsorption geometries are presented in Fig. 13. It can be seen that the three-fold adsorption is accompanied by low density of *z*-polarized vibrational modes localized on adatoms and the surface layer atoms of the substrate. The highest peaks of the density of states of these modes appear at energies of 18.3–19.4 meV. A low-frequency region exhibits an intense peak of adatom translational displacements. These displacements give rise to states in the substrate surface layers that were missing in the case of the clean aluminium surface and that coincide in energy with the mode of adatom translational displacements. The intensity of peaks corresponding to the characteristic vibrations of clean surface atoms decreases several-fold.

A different pattern of vibrational state distribution is observed for sodium in six-fold substitutional adsorption sites. In the region of 11.5–12.5 meV, an intense peak of Z-vibrations of adatoms and substrate surface layer atoms is detected. The Z-vibrations of atoms of the second surface layer of the substrate occur in the same region. The surface layer atoms execute vibrations in the sagittal plane at these energy values. In the low-frequency region, a peak for translational displacements is missing, which is indicative of stronger interactions of the adatoms with the substrate and of more stable state of the $(\sqrt{3}\times\sqrt{3})$R30°–Na structure on the aluminium surface. Comparison with the state density distribution for clean Al(111) surface showed that the presence of sodium adatoms induces a low-frequency shift of the Rayleigh mode, and the high-frequency shear vibrations shift to the upper boundary of the bulk phonon region. All vibrations of the surface layer atoms are suppressed and low-frequency vertical and high-frequency longitudinal vibrations of atoms in the subsurface layers of the substrate are enhanced.

Thus, the EAM calculation of the vibrational characteristics of the sodium adsorption on the Al(111) surface in different adsorption positions demonstrated substantial softening of the translational mode of the adsorbate and weak adatom–substrate interaction in the case of adatom-type adsorption. Also, the substitutional adsorption is accompanied by strengthening of the Na–Al bonds and weakening of Na–Na interactions, and by increase in the vertically polarized vibrational state density due to coupled vibrations of adatoms and substrate atoms. All this makes it possible, together with structural studies, to interpret metastable and irreversible nature of low-temperature adsorption from the dynamic standpoint.

c. Effect of the coverage on the phonon spectrum

The effect of the adsorbate coverage on the vibrational properties of adsorption systems was studied in relation to the Na–Cu(111) systems. It was found experimentally [67, 68, 183–190] and theoretically [54, 75, 76, 191, 192] that submonolayer adsorption of alkali metal atoms on the Cu(111) surface, up to a saturated monolayer ($\theta = 0.44$), where adatoms form a hexagonal structure, $(3/2\times3/2)$, gives rise to rows of ordered p(3×3), p(2×2), p$(\sqrt{3}\times\sqrt{3})$ structures at coverages $\theta = 0.11$, 0.25 and 0.33, respectively. The calculation of the bond energy for the equilibrium geometry of the p(2×2) structure demonstrated that all sodium atoms are located strictly above the three-fold FCC cavities of the substrate.[186] For the $(3/2\times3/2)$ structure, non-equivalence of adsorption sites was found in the same work: one adatom is located strictly above the three-fold FCC cavity, while the other three adatoms are displaced from these sites. The structures with $(3/2\times3/2)$, p(3×3) and p$(\sqrt{3}\times\sqrt{3})$ periodicities correspond to the (3×3) unit cell, while for p(2×2), the unit cell dimension is (2×2). The Brillouin zones corresponding to the described structures are presented in Fig. 14. As a result of BZ collapse, the symmetrical points are reflected by the following rule:

(3×3)

$\overline{\Gamma} \leftarrow \overline{K}, 2/3\,\overline{\Gamma}\,\overline{M}, \overline{K}' \leftarrow 1/3\,\overline{\Gamma}\,\overline{K}, 2/3\,\overline{\Gamma}\,\overline{K}, 1/3\,\overline{K}\,\overline{M};$

(2×2)

$\overline{\Gamma} \leftarrow \overline{M}, \overline{K}' \leftarrow 1/2\,\overline{\Gamma}\,\overline{K}, \overline{M}' \leftarrow \overline{M}, 1/2\,\overline{\Gamma}\,\overline{K}, 1/3\,\overline{\Gamma}\,\overline{K},$

$\overline{M}' \leftarrow 1/2\,\overline{\Gamma}\,\overline{M}, 3/4\,\overline{\Gamma}\,\overline{K}$

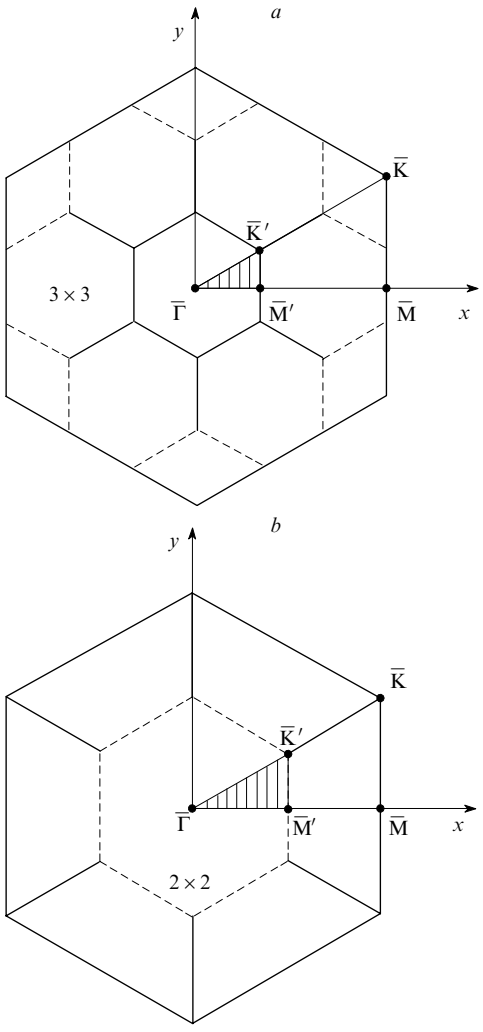


Figure 14. Brillouin zone of surface superstructures p(3×3), p$(\sqrt{3}\times\sqrt{3})$, $(3/2\times3/2)$ (*a*) and p(2×2) (*b*).[54]
The irreducible parts of BZ of the (3×3) and (2×2) structures are dashed; the continuous line shows the Brillouin zone corresponding to the (1×1) structure.

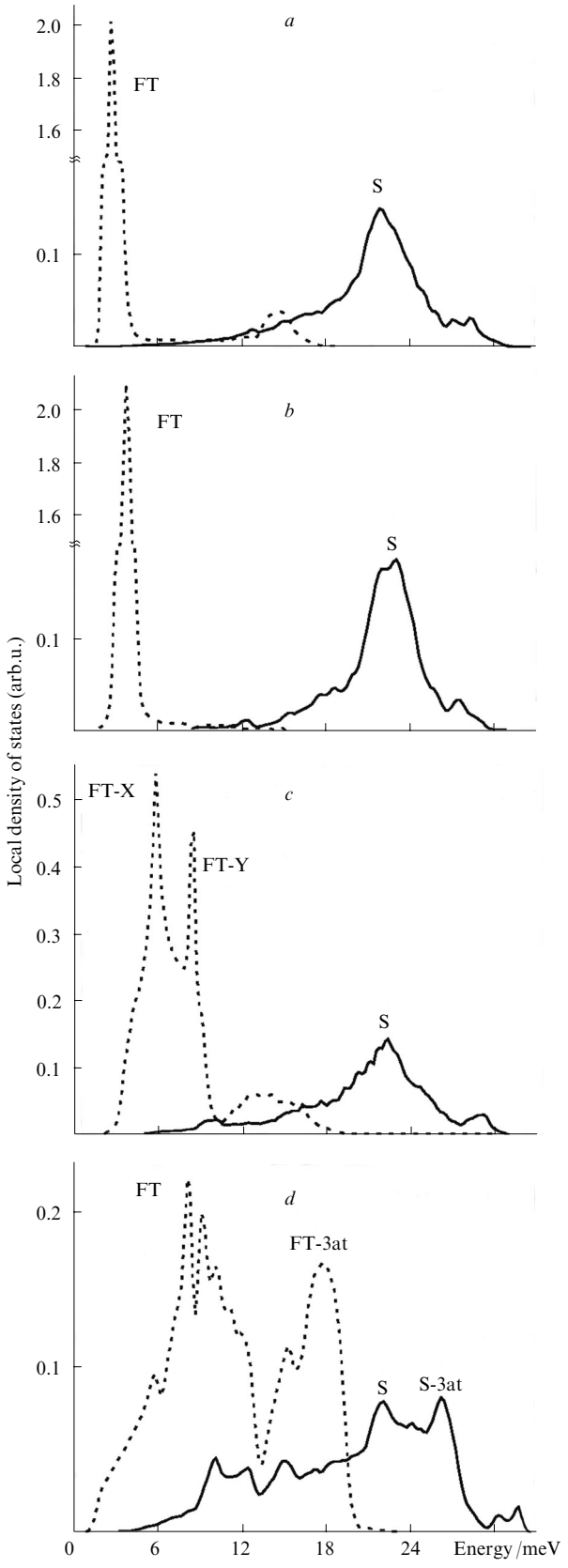


Figure 15. Density distribution of the phonon states on the adatoms for the Cu(111)–p(3×3)–Na (*a*), Cu(111)–p(2×2)–Na (*b*), Cu(111)–($\sqrt{3}\times\sqrt{3}$)R30°–Na (*c*) and Cu(111)–(3/2×3/2)–Na (*d*) systems.[56]
FT-3at and S-3at are the modes for three displaced adatoms.

The energy of the S mode upon sub-monolayer adsorption was measured[68] using EELS for the Na/Cu(111) system. The resulting value of 21 meV remained invariable at any coverages. However, the peak intensity corresponding to this mode depended on the coverage at low coverages ($\theta = 0.016-0.2$) and was maximum at $\theta = 0.15$. At $\theta \geqslant 0.25$ monolayers, the intensity was constant and retained its value up to monolayer saturation. *Ab initio* calculation also gave the S-mode energy of 21 meV.[186] The equilibrium crystal structure and the vibrational properties of the Na/Cu(111) system were studied in detail at different coverages.[54] All of the surface modes of the clean Cu(111) surface were found to be retained; however, they have coupled vibrations and frequency shifts caused by the interaction with adatoms. The calculated S-mode energy was 22 meV for any coverage; it is in line with experimental data.[68] The invariability of the S-mode energy is clearly seen in the vibrational state density distribution on adatoms (Fig. 15).

Ananylsis of the phonon state density demonstrated that the S-mode energy does not depend on the coverage. However, the coverage has a considerable influence on the FT mode: this influence increases by a factor of three on going from $\theta \approx 0.11$ to $\theta \approx 0.44$. As the coverage increases, the density of adatoms in the layer grows, resulting in stronger interaction between the atoms, which is responsible for the FT mode. Experimental investigations of the vibrational characteristics of a multilayer sodium film on the Cu(100) surface showed[189,190] that at a 20 monolayer-thick adsorption film, the FT mode transforms into a longitudinal surface mode of neat sodium. When the coverage is 0.44 corresponding to a saturated sodium monolayer, the spectrum of the local density of vibrational states shows S mode splitting. The splitting is caused by non-equivalence of the adsorption sites resulting from the structural mismatch of the monolayer film and the substrate. The effect of adatoms on the vibrational properties of the substrate is manifested as excitation of new *z*-polarized modes in both the low-frequency and high-frequency regions of the phonon spectrum of the substrate. The excitation energy of the transverse S mode, which represents coupled vibrations of adatoms and substrate atoms is higher than the energy of the FT mode of coupled translations of the adsorbate atoms (see Figs 15 and 12). This energy ratio of the vibrational modes of the adsorbate, as in the case of sodium adsorption in the three-fold sites on the Al(111) surface, corresponds to weak adatom–substrate interaction and metastable nature of sodium adsorption on the Cu(111) surface.

d. Effect of the crystallographic orientation of the substrate surface on the phonon spectrum

Clean metal surfaces tend to show anisotropy of atomic vibrations in the directions perpendicular and parallel to these surfaces.[63,64] In addition, the anisotropy of displacements along the [001] and [110] directions exists in the (110) surface, resulting from different atomic environments along these directions. By studying the adsorption of adatoms of one metal on simple surfaces of another metal, it is possible to identify the effect of substrate anisotropy on the dynamic stability of adsorption systems, which is determined by the FT to S mode ratio. The experimental and theoretical data on the vibrational characteristics of various adsorption systems were described systematically.[56,69,134] Based on these data and results of EAM calculations, the role of

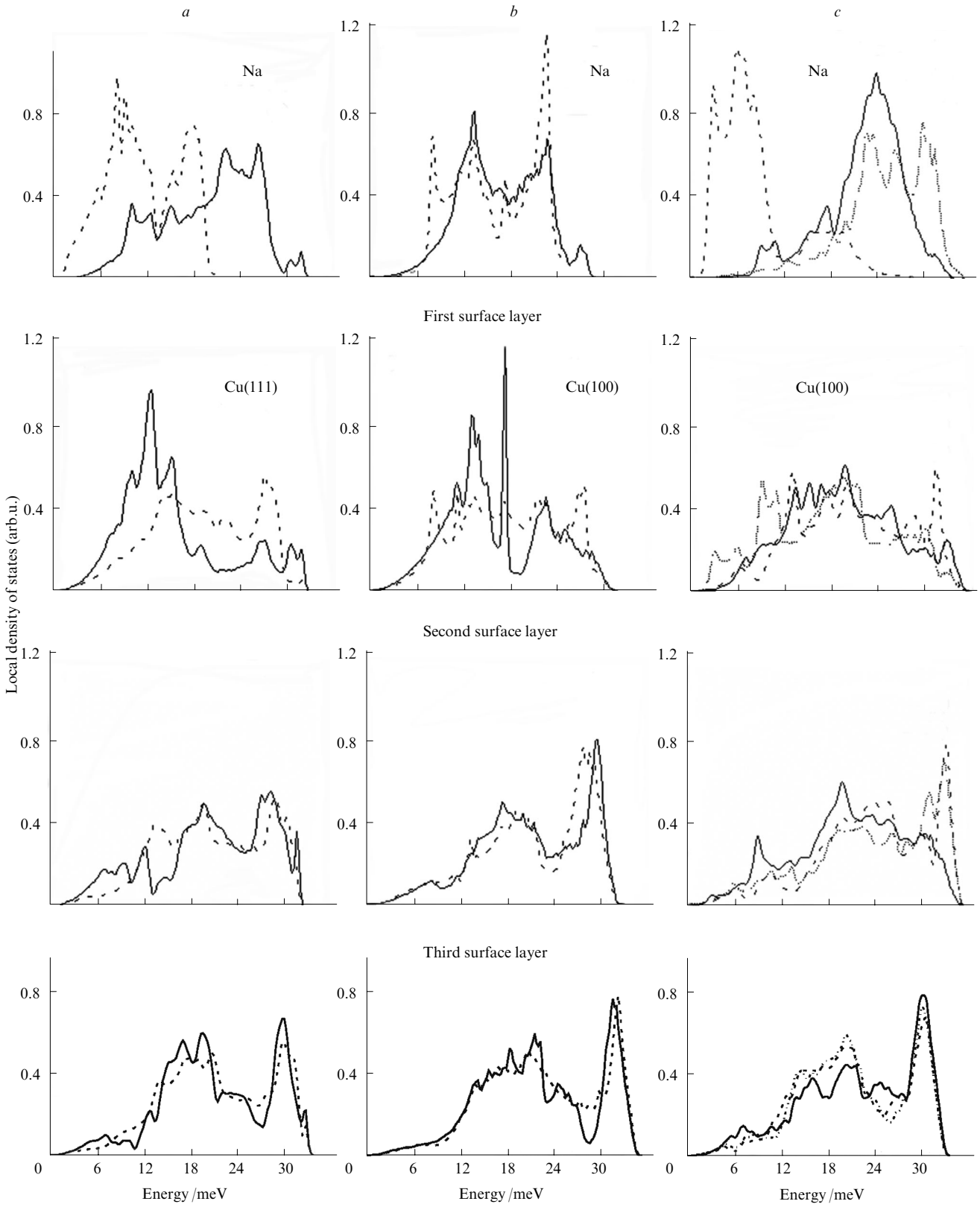


Figure 16. Local state densities for the Cu(111) (*a*), Cu(100) (*b*) and Cu(110) (*c*) surfaces with adsorbed sodium.[54, 134]
The coverage corresponds to a saturated monolayer; dash-and-dot, dash and continuous lines are the *x*-, *y*- and *z*-polarized states, respectively.

substrate orientation was considered in relation to the Na–Cu system. Experimental investigations of sodium adsorption on simple copper surfaces demonstrated [67, 183–188, 191–199] that atoms are always adsorbed according to the adatom type above the three-fold vacancies. This is due to the ratio of the adatom radius and the interatomic distances in the substrate. The adsorption of sodium on any of the considered copper surfaces gives rise to relaxation effects: the first interlayer spacings are shortened and rippling of the structure in the subsurface layers occurs.[180] The coverage corresponding to a saturated sodium monolayer is 0.44 for the (111) surface and 0.5 for the (100) and (110) surfaces. This gives rise to a structure with periodicity of $(3/2 \times 3/2)$, $c(2 \times 2)$ and (2×1), respectively.

The effect of substrate orientation can be followed by considering the distribution of vibrational states over the atomic layers. The local densities of states for the adsorption of sodium on the copper (111), (100) and (110) surfaces are shown in Fig. 16. The splitting of localized peaks corresponding to FT modes (*xy*-polarization) and S modes (*z*-polarization) is characteristic of the (111) and (100) surfaces. In the case of the (111) surface, this splitting is due to non-equivalence of adsorption sites, some atoms being adsorbed strictly in the three-fold sites, while other adatoms are displaced from these sites. In the case of the (100) surface, splitting is related to non-equivalence of the surrounding by substrate atoms along the [100] and [110] directions. This behaviour of the modes on the (100) surface is consistent with the experimental data.

Kliewer and Berndt [67] found the anisotropy of interatomic interactions along the directions that coincide with $\bar{\Gamma}\bar{M}'$ and $\bar{\Gamma}\bar{X}'$ of the two-dimensional BZ of the adsorption structure. The energy of the S mode of adatoms located strictly in three-fold adsorption sites is invariable for both surfaces being equal to $\sim$22 meV. The anisotropy of adatom vibrations (the wave vector **q** of which is directed along [100]) is most pronounced for the (110) surface. In this case, considerable splitting of the FT mode is observed. The *x*-polarized FT mode caused by displacement along the [100] direction (perpendicular to rows of adatoms) has a very low vibrational energy ($\sim$6 meV). Meanwhile, the energy of the *y*-polarized FT mode caused by displacements along the $[\bar{1}10]$ direction (along the rows of adatoms) sharply increases ($\sim$26 meV) and is located above the energy of the S mode. The peak corresponding to the S mode has a pronounced localized nature and falls into the energy gap between *x*- and *y*-polarized branches of the FT mode. The energy of this mode, as in previous cases, is $\sim$22 meV. The appearance of the soft mode along the [100] direction attests to structural instability of the system along this direction. Experimental investigation showed [198, 199] that at a coverage of 0.14, sodium adatoms already induce missing-row reconstruction of the (2×1) Cu(110) surface. The experimental [199] value of the energy of low-frequency part of the FT mode, 5.4 meV, is consistent with the calculated value (6 meV).

Comparative analysis of the energy ratio of the FT and S modes provides the conclusion that the most stable adsorption structure is formed on the (100) surface for which the energy balance of these modes, which fall in the same energy range, is observed. Force constant analysis demonstrated that the Na–Na interaction only slightly ($\sim$15%) predominates over $Na-Cu_1$. The adsorption structure on the (111) surface is the least dynamically stable because in this case, the excitation energy of the FT mode is much lower than the excitation energy of the S mode, which reflects its migrational instability. This conclusion is also supported by the degree of modification of the vibrational characteristics of the substrate surface layer. Sodium adsorption on the (111) surface induces a minor high-frequency shift of the Rayleigh mode and gives rise to additional high-frequency *z*-polarized vibrations (see Fig.16 *a*), while the adsorption on the (100) surface leads to splitting of the Rayleigh mode of the substrate and increase in its energy from 15.3 to 17.1 meV. The energy of longitudinal vibrations of surface atoms of the substrate decreases.

The most pronounced effect on the vibrational properties of the surface layer of the substrate is exerted by adsorption on the Cu(110) surface: the Rayleigh mode of the substrate is suppressed and the energy of longitudinal vibrations decreases. However, unlike the (111) and (100) surfaces, the adsorption leads to excitation, in the subsurface layer, of *z*-polarized vibrational modes, which are absent in the case of clean surface. The appearance of these modes attests to strong interaction of the adatoms with the second layer. As it was shown above for clean surfaces, this type of vibrations is inherent in the Pd(110) surface but not in clean Cu(110) surface.

V. Conclusion

This review considers the state of the art studies of the dynamics of metallic surfaces. We endeavoured to present data on surface phonons as fully as possible. Also, taking the embedded atom method as an example, we demonstrated the efficiency of using model methods for the theoretical description of the structure of metal surfaces and the type of surface atom vibrations, in particular, in the presence of structural defects or adatoms. The comparative analysis showed that the use of such methods provides not only qualitative but also quantitative agreement with *ab initio* calculations and experimental data. Undoubtedly, this simplifies calculations for complex surface systems, extends the possibilities of further investigations along important lines of research of surface physics and chemistry (for example, the dynamics and stability of surface clusters, interfaces and inner boundaries, in particular, grain boundaries in polycrystalline materials,[51, 200] atom diffusion and migration over the surface [201]) and helps to describe the electron–phonon interaction on the surface.[202] The analysis of numerous publications devoted to the effect of various factors on the formation of the surface phonon structure and its evolution upon complication of the surface geometry or in the presence of adatoms provides the following conclusions.

In the case of metals that refer to the same structural group (*e.g.*, FCC), the phonon spectra of both simple and vicinal surfaces are determined by the surface geometry and are qualitatively similar irrespective of the chemical type of the metal. The difference is manifested in the energies of phonon modes, which are affected by surface force constants and the degree of surface relaxation. The relaxation gives rise to an additional low-frequency resonance-type longitudinal mode, which is absent in an ideal surface. The presence of steps accounts for the change in the phonon structure of the surface — appearance of new type of vibrational modes, so-called step modes, which are mainly localized in the step and do not get to the terrace.

For all adsorption systems, irrespective of the chemical type of the adsorbate and substrate, the phonon spectrum always exhibits two characteristic hybridized vibrational modes, which are largely localized on adatoms and are caused by adatom – adatom and adatom – substrate interactions. Upon adatom sub-monolayer adsorption on metal surfaces, the adatom – adatom interaction gives rise to a low-frequency mode of coupled frustrated translations (FT mode) in the phonon spectrum; this mode determines the migration of adsorbed atoms over the substrate surface. The adatom – substrate interaction is manifested in the phonon spectrum as a stretching S mode polarized strictly perpendicular to the surface. This mode is largely responsible for the desorption stability of adatoms on the substrate surface. As the coverage increases, the energy of the S mode remains almost invariable, while the energy of the FT mode increases.

The sub-monolayer adsorption on the (110) surface of FCC metals brings about a substantial anisotropy of the transverse displacements of adatoms. The longitudinal FT mode is split into *x*- and *y*-polarized modes, which propagate across and along the adatom row, respectively. In the phonon spectrum of the substrate, the density of the shear modes localized in the surface layer and coinciding in polarization with the *x*-polarized mode of the FT adsorbate increases. In the subsurface layer, there is a highly localized vertical mode, which propagates in the sagittal plane and is coupled with analogous vibrations of adatoms. It was shown experimentally that even a minor coverage ($\theta \leqslant 0.15$ monolayers) of the Cu(110) surface by the alkali metal induces the missing-row reconstruction, which occurs along *x*-polarization of the FT mode. The theoretically calculated behaviour of atomic vibrations upon the adsorption of alkali metals on the Cu(110) surface suggests the presence of a dynamic component of this reconstruction.

In the case of sub-monolayer adsorption, the vibrational spectrum of the substrate is modified: a frequency shift of the surface modes occurs, the degree of localization of vibrations on the surface layer decreases and new vibrational modes untypical of a clean surface arise.

The authors are sincerely grateful for longstanding cooperation and fruitful discussion of the results to Ph.Ds in physics and mathematics S D Borisova and I Yu Sklyadneva, Doctor of Sciences in physics and mathematics S V Eremeev (Institute of Strength Physics and Materials Science, Siberian Branch of the Russian Academy of Sciences), Doctors T Nagao (National Institute for Materials Science, Tsukuba, Japan) and R Heid (Karlsruhe Institute of Technology, Germany), Professors P M Echenique (Department of Condensed Matter Physics, University of the Basque Country, Spain), G Benedek (University of Milono-Bicocca, Milan, Italy) and K P Bohnen (Forschungszentrum Karlsruhe, Institut für Festkorperphysik, Germany).

References

1. I M Lifshits, L N Rozentsveig *Zh. Eksp. Teoret. Fiz.* **18** 1012 (1948)
2. A A Maradudin, E W Montroll, G H Weiss, I P Ipatova *Theory of Lattice Dynamics in the Harmonic Approximation* (New York: Academic Press, 1971)
3. J Frisch, U Schröder *Phys. Rep.* **309** 209 (1999)
4. R Heid, K-P Bohnen *Phys. Rep.* **387** 151 (2003)
5. T S Rahman, A Kara, S J Durukanoglu *J. Phys.: Condens. Matter* **15** S3197 (2003)
6. Lord Rayleigh *Proc. Lond. Math. Soc.* **17** 4 (1887)
7. A E H Love *Some Problems of Geodynamics* (London: Cambridge University Press, 1911)
8. R Stoneley *Proc. R. Soc. London, Ser. A* **106** 416 (1924)
9. R F Wallis *Phys. Rev.* **105** 540 (1957)
10. R E Allen, G P Alldredge, F W De Wette *Phys. Rev. B* **4** 1648 (1971)
11. R E Allen, G P Alldredge, F W De Wette *Phys. Rev. B* **4** 1661 (1971)
12. G P Alldredge, R E Allen, F W De Wette *Phys. Rev. B* **4** 1682 (1971)
13. R B Doak, U Harten, J P Toennies *Phys. Rev. Lett.* **51** 578 (1983)
14. J P Toennies, in *Surface Phonons* (Eds W Kress, F W De Wette) (Berlin: Springer, 1991)
15. G Benedek, J P Toennies *Surf. Sci.* **299 – 300** 587 (1994)
16. H Ibach, D I Mills *Electron Energy Loss Spectroscopy and Surface Vibrations* (New York: Academic Press, 1982)
17. G Benedek, J Ellis, N S Luo, A Reichmuth, P Ruggerone, J P Toennies *Phys. Rev. B* **48** 4917 (1993)
18. G Benedek, L Miglio, G Brusdeylins, J G Skofronick, J P Toennies *Phys. Rev. B* **35** 6593 (1987)
19. U Harten, J P Toennies, C Woll *Phys. Rev. Lett.* **57** 2947 (1986)
20. R B Doak, D B Nguyen *J. Electron Spectrosc. Relat. Phenom.* **44** 205 (1987)
21. H Ibach *Phys. Rev. Lett.* **27** 253 (1971)
22. H M Mohamed, L L Kesmodel *Phys. Rev. B* **37** 6519 (1988)
23. Y Chen, S Y Tong, J-S Kim, L L Kesmodel, T Rodach, K-P Bohnen, K M Ho *Phys. Rev. B* **44** 11394 (1991)
24. H Nienhaus, S P Grabowski, W Mönch *Phys. Status Solidi A* **159** 175 (1997)
25. M Balden, S Lehwald, H Ibach *Phys. Rev. B* **53** 7479 (1996)
26. O L Alerhand, E J Mele *Phys. Rev. B* **37** 2537 (1988)
27. U Del Pennino, C Mariani, A Amaddeo, R Biagi, F Proix, C Sébeme *J. Phys.: Condens. Matter* **5** 6613 (1993)
28. *Inelastic Electron Tunneling Spectroscopy* (Ed. T Wolfram) (Berlin: Springer, 1978)
29. R J Hamers, R M Tromp, J E Demuth *Phys. Rev. Lett.* **56** 1972 (1986)
30. L Vitali, S D Borisova, G G Rusina, E V Chulkov, K Kern *Phys. Rev. B* **81** 153409 (2010)
31. M Born, K Huang *Dynamical Theory of Crystal Lattices* (Oxford: Clarendon Press, 1954)
32. J K Norskov, N D Lang *Phys. Rev. B* **21** 2131 (1980)
33. M S Daw, M I Baskes *Phys. Rev. B* **29** 6443 (1984)
34. F Cleri, V Rosato *Phys. Rev. B* **48** 22 (1993)
35. R F Wallis, in *Progress in Surface Science* Vol. 4 (Oxford: Pergamon Press, 1973) p. 233
36. J E Black, D A Campbell, R F Wallis *J. Phys.* **42** 837 (1981)
37. J E Black, F C Shanes, R F Wallis *Surf. Sci.* **133** 199 (1983)
38. J E Black, R F Wallis *Phys. Rev. B* **29** 6972 (1984)
39. C T Chan, K-P Bohnen, K M Ho *Phys. Rev. Lett.* **69** 1672 (1992)
40. J Cai, Y Y Ye *Phys. Rev. B* **54** 8398 (1996)
41. M S Daw, R L Hatcher *Solid State Commun.* **56** 697 (1985)
42. J S Nelson, E C Sowa, M S Daw *Phys. Rev. Lett.* **61** 1977 (1988)
43. E V Chulkov, I Yu Sklyadneva *Surf. Sci.* **331 – 333** 1414 (1995)
44. S Durukanoglu, T S Rahman *Surf. Sci.* **409** 395 (1998)

45. I Yu Sklyadneva, G G Rusina, E V Chulkov *Surf. Sci.* **377 – 379** 313 (1998)
46. G G Rusina, A V Berch, I Yu Sklyadneva, S V Eremeev, A G Lipnitskii, E V Chulkov *Fiz. Tv. Tela* **38** 1120 (1996) [a]
47. I Yu Sklyadneva, G G Rusina, E V Chulkov *Surf. Sci.* **416** 17 (1998)
48. I Yu Sklyadneva, G G Rusina, E V Chulkov *Phys. Rev. B* **65** 235419 (2002)
49. I Yu Sklyadneva, G G Rusina, E V Chulkov *Phys. Rev. B* **68** 045413 (2003)
50. G G Rusina, I Yu Sklyadneva, E V Chulkov *Thin Solid Films* **228** 27 (1993)
51. I Yu Sklyadneva, G G Rusina, E V Chulkov *Surf. Sci.* **433 – 435** 517 (1999)
52. G G Rusina, S D Borisova, S V Eremeev, I Yu Sklyadneva, E V Chulkov *Izv. Vussh. Ucheb. Zaved, Fiz.* **11** 49 (2004) [b]
53. G G Rusina, S D Borisova, S V Eremeev, I Yu Sklyadneva, E V Chulkov *Phys. Rev. B* **71** 245401 (2005)
54. S D Borisova, G G Rusina, S V Eremeev, G Benedek, P M Echenique, I Yu Sklyadneva, E V Chulkov *Phys. Rev. B* **74** 165412 (2006)
55. G G Rusina, S D Borisova, S V Eremeev, I Yu Sklyadneva, E V Chulkov *Surf. Sci.* **600** 3921 (2006)
56. G G Rusina, S V Eremeev, P M Echenique, S D Borisova, G Benedek, E V Chulkov *J. Phys.: Condens. Matter* **19** 266005 (2007)
57. G G Rusina, S D Borisova, S V Eremeev, E V Chulkov *Fiz. Tv. Tela* **50** 1510 (2008) [a]
58. J E Black, P Bopp *Surf. Sci.* **140** 275 (1984)
59. P Knipp *Phys. Rev. B* **43** 6908 (1991)
60. S Durukanoglu, A Kara, T S Rahman *Phys. Rev. B* **55** 13894 (1997)
61. R Heid, A Kara, K-P Bohnen, T S Rahman *Phys. Rev. B* **65** 115405 (2002)
62. S Y Wie, S P Lewis, E J Mele, A M Rappe *Phys. Rev. B* **57** 10062 (1998)
63. G Benedek, J Ellis, A Reichmuth, P Ruggerone, H Shief, J P Toennies *Phys. Rev. Lett.* **69** 2951 (1992)
64. P Senet, J P Toennies, G Witte *Chem. Phys. Lett.* **299** 389 (1999)
65. J Ellis, A P Graham, F Hofmann, J P Toennies *Phys. Rev. B* **63** 195408 (2001)
66. D L Adler, I R Collins, X Liang, S J Murray, G S Leatherman, K-D Tsuei, E E Chaban, S Chandavarkar, R McGrath, R D Diehl, P H Citrin *Phys. Rev. B* **48** 17445 (1993)
67. J B Kliewer, R Berndt *Surf. Sci. B* **477** 250 (2001)
68. S-A Lindgren, C Svensson, L Walldén *Phys. Rev. B* **42** 1467 (1990)
69. S E Finberg, J V Lakin, R D Diehl *Surf. Sci.* **496** 10 (2002)
70. R D Diehl, R McGrath *Surf. Sci. Rep.* **23** 43 (1996)
71. H Tochihara, S Mizuno *Prog. Surf. Sci.* **58** 11 (1998)
72. L A Bol'shov, A P Napartovich, A G Naumovets, A G Fedorus *Physics-Uspekhi* **20** 432 (1977)
73. E V Chulkov, V M Silkin *Surf. Sci.* **215** 385 (1989)
74. B Hellsing, A Eiguren, E V Chulkov *J. Phys.: Condens. Matter* **14** 5959 (2002)
75. E V Chulkov, J Kliewer, R Berndt, V M Silkin, B Hellsing, S Crampin, P M Echenique *Phys. Rev. B* **68** 195422 (2003)
76. B Hellsing, J Carlsson, L Walldén, S-E Lindgren *Phys. Rev. B* **61** 2343 (2000)
77. A G Borisov, J P Gauyacq, E V Chulkov, V M Silkin, P M Echenique *Phys. Rev. B* **65** 235434 (2002)
78. J Zhao, N Pontius, A Winkelmann, V Sametoglu, A Kubo, A G Borisov, D Sánchez-Portal, V M Silkin, E V Chulkov, P M Echenique, H Petek *Phys. Rev. B* **78** 085419 (2008)
79. C Corriol, V M Silkin, D Sanchez-Portal, A Arnau, E V Chulkov, P M Echenique, T von Hofe, J Kliewer, J Kröger, R Berndt *Phys. Rev. Lett.* **95** 176802 (2005)
80. E V Chulkov, A G Borisov, J P Gauyacq, D Sánchez-Portal, V M Silkin, V P Zhukov, P M Echenique *Chem. Rev.* **106** 4160 (2006)
81. *Physics and Chemistry of Alkali Metal Adsorption* (Amsterdam: Elsevier, 1989)
82. H Ishida, K Terakura *Phys. Rev. B* **38** 5752 (1988)
83. J Neugebauer, M Scheffler *Phys. Rev. B* **46** 16067 (1992)
84. M Scheffler, C Stampfl, in *Handbook of Surface Science. Electronic Structure* Vol. 2 (Amsterdam: Elsevier, 1999) p. 286
85. T Nagao, Y Iizuka, M Umeuchi, T Shimazaki, C Oshima *Surf. Sci.* **329** 269 (1995)
86. J N Andersen, M Ovarford, R Nyholm, J F Van Acker, E Lundgren *Phys. Rev. Lett.* **68** 94 (1992)
87. J N Andersen, E Lundgren, R Nyholm, M Qvarford *Surf. Sci.* **289** 307 (1993)
88. M Born, R Oppenheimer *Ann. Phys.* **84** 457 (1927)
89. B C Clark, R Herman, R F Wallis *Phys. Rev. A* **139** 860 (1965)
90. W Kohn, L J Sham *Phys. Rev. B* **140** A1133 (1965)
91. P Hohenberg, W Kohn *Phys. Rev. B* **136** 864 (1964)
92. S Yu Savrasov, E G Maksimov *Physics-Uspekhi* **38** 737 (1995)
93. S Baroni, S De Gironcoli, A Dal Corso *Rev. Mod. Phys.* **73** 515 (2001)
94. S V Eremeev, A I Potekaev *Izv. Vussh. Ucheb. Zaved, Fiz.* **48** 82 (2005) [b]
95. A G Lipnitskii Candidate Thesis in Physical and Mathematical Sciences, Institute of Strength Physics and Materials Science of the Siberian Branch of the Russian Academy of Sciences, Tomsk, 1989
96. S M Foiles, M I Baskes, M S Daw *Phys. Rev. B* **33** 7983 (1986)
97. S M Foiles *Phys. Rev. B* **32** 7685 (1985)
98. R S Jones *Phys. Rev. B* **41** 3256 (1990)
99. J H Rose, J R Smith, F Guinea, J Ferrante *Phys. Rev. B* **29** 2963 (1984)
100. R A Johnson *Phys. Rev. B* **16** 2094 (1972)
101. *American Institute of Physics Handbook* (Ed. D E Gray) (New York: McGraw-Hill, 1972)
102. H L Davis, J Nooman *Surf. Sci.* **126** 45 (1983)
103. I Stenagaard, L R Feidenhans, J E Sorensen *Surf. Sci.* **128** 281 (1983)
104. R N Barnett, V Landman, C L Cleveland *Phys. Rev. B* **27** 6534 (1983)
105. R D Diehl, M Lindroos, A Kearsley, C J Barnes, D A King *J. Phys.* **18** 4069 (1985)
106. M A Vasil'ev *Struktura i Dinamika Poverkhnosti Perekhodnykh Metallov* (Structure and Dynamics of Transition Metal Surfaces) (Kiev: Naukova Dumka, 1988)
107. P R Watson, K A R Mitchell *Surf. Sci.* **203** 323 (1988)
108. G Witte, J Braun, A Lock, J P Toennies *Phys. Rev. B* **52** 2165 (1995)
109. T Rodach, K-P Bohnen, K M Ho *Surf. Sci.* **209** 481 (1989)
110. S B Sinnott, M S Stave, T J Raeker, A E DePristo *Phys. Rev. B* **44** 8927 (1991)
111. Ph Hofmann, I Yu Sklyadneva, E D L Rienks, E V Chulkov *New J. Phys.* **11** 125005 (2009)

112. V Chis, B Hellsing, G Benedek, M Bernasconi, E V Chulkov, J P Toennies *Phys. Rev. Lett.* **101** 206102 (2008)
113. V Rosato, M Guillope, B Legrand *Philos. Mag. A* **59** 321 (1989)
114. I Yu Sklyadneva, G Benedek, E V Chulkov, P M Echenique, R Heid, K-P Bohnen, J P Toennies *Phys. Rev. Lett.* **107** 095502 (2011)
115. A Leonardo, I Yu Sklyadneva, V M Silkin, P M Echenique, E V Chulkov *Phys. Rev. B* **76** 035404 (2007)
116. E V Chulkov, I Yu Sklyadneva, G G Rusina *Fiz. Met. Metalloved.* **75** 42 (1993) [c]
117. G G Rusina, I Yu Sklyadneva, A V Polubyatko, E V Chulkov *Poverkhnost'* (3) 9 (1993)
118. A V Bertsch, E V Chulkov, A G Lipnitskii, I Yu Sklyadneva, G G Rusina *Phys. Low-Dim. Struct.* **4 – 5** 95 (1994)
119. A V Bertsch, E V Chulkov, S V Eremeev, A G Lipnitskii, G G Rusina, I Yu Sklyadneva *Vacuum* **46** 625 (1995)
120. I Yu Sklyadneva, E V Chulkov, A V Bertsch *Surf. Sci.* **352 – 354** 25 (1996)
121. G G Rusina, I Yu Sklyadneva, E V Chulkov *Fiz. Tv. Tela* **38** 1483 (1996) [a]
122. G G Rusina, I Yu Sklyadneva, E V Chulkov *Phys. Low-Dim. Struct.* **9 – 10** 127 (2001)
123. I Yu Sklyadneva, G G Rusina, S V Eremeev, E V Chulkov *Phys. Low-Dim. Struct.* **1 – 2** 115 (2003)
124. G Benedek, J P Toennies *Surface Science: the First Thirty Years* (Ed. C B Duke) (Amsterdam: North-Holland, 1994)
125. C Calandra, A Catellani, C Beatrice *Surf. Sci.* **148** 90 (1984)
126. A Franchini, V Bortolani, G Santoro, J F Gaspar, A G Eguiluz *Surf. Sci.* **269 – 270** 146 (1992)
127. I Yu Sklyadneva, R Heid, K-P Bohnen, E V Chulkov *New J. Phys.* **11** 103038 (2009)
128. I Yu Sklyadneva, R Heid, K-P Bohnen, P M Echenique, E V Chulkov *J. Phys.: Condens. Matter* **24** 104004 (2012)
129. L Yang, T S Rahman, M S Daw *Phys. Rev. B* **44** 13725 (1991)
130. I Yu Sklyadneva, R Heid, K-P Bohnen, P M Echenique, G Benedek, E V Chulkov *J. Phys. Chem. A* **115** 7352 (2011)
131. Th Rodach, K-P Bohnen, K M Ho *Surf. Sci.* **296** 123 (1993)
132. Y Chen, S Y Tong, K-P Bohnen, T Rodach, K M Ho *Phys. Rev. Lett.* **70** 603 (1993)
133. M Rocca *Surface Phonon Dispersion* (Berlin: Springer, 2002)
134. G G Rusina, Doctoral Thesis in Physical and Mathematical Sciences, Institute of Strength Physics and Materials Science of the Siberian Branch of the Russian Academy of Sciences, Tomsk, 2010
135. M Balden, S Lehwald, H Ibach, A Ormeci, D L Mills *Phys. Rev. B* **46** 4172 (1992)
136. P Zeppenfeld, K Kern, R David, K Kuhnke, G Gomsa *Phys. Rev. B* **38** 12329 (1988)
137. Y Chen, S Y Tong, M Rocca, P Moretto, U Valbusa, K-P Bohnen, K M Ho *Surf. Sci. Lett.* **250** L389 (1991)
138. A M Lahee, J P Toennies, C A Wöll *Surf. Sci.* **191** 1529 (1987)
139. S Andersson, J B Pendry, P M Echenique *Surf. Sci.* **65** 539 (1977)
140. C Calandra, A Catellani, C Beatrice *Surf. Sci.* **152** 814 (1985)
141. K-P Bohnen *Surf. Sci.* **147** 304 (1984)
142. B Lang, R W Joyner, A Somorjai *Surf. Sci.* **30** 454 (1972)
143. P Jiang, F Jona, P M Marcus *Phys. Rev. B* **35** 7952 (1987)
144. S Durukanoglu, T S Rahman *Phys. Rev. B* **67** 205406 (2003)
145. D Spisak *Surf. Sci.* **489** 151 (2001)
146. J L F Silva, K Schroeder, S Blügel *Phys. Rev. B* **72** 033405 (2005)
147. J L F Silva, K Schroeder, S Blügel *Surf. Sci.* **600** 3008 (2006)
148. W T Geng, A J Freeman *Phys. Rev. B* **64** 115401 (2001)
149. S R Parkin, P R Watson, R A McFarlane, K A R Mitchell *Solid State Commun.* **78** 841 (1991)
150. T Seyller, R D Diehl, F J Jona *Vac. Sci. Technol. A* **17** 1635 (1999)
151. Y Tian, K-W Lin, F Jona *Phys. Rev. B* **62** 12844 (2000)
152. I S Chandravakar, D M Zehner *Surf. Sci.* **504** L201 (2002)
153. D A Walko, I K Robinson *Phys. Rev. B* **59** 15446 (1999)
154. S Walter, H Baier, M Weinelt, K Heinz, T Fauster *Phys. Rev. B* **63** 155407 (2001)
155. M Lischka, A Groß *Phys. Rev. B* **65** 075420 (2002)
156. I Makkonen, P Salo, M Alatalo, S Rahman *Phys. Rev. B* **67** 165415 (2003)
157. D L Adams, C S Sorensen *Surf. Sci.* **166** 495 (1986)
158. D L Adams, V Jensen, X F Sun, J H Vollesen *Phys. Rev. B* **38** 7913 (1988)
159. J R Noonan, H L Davis, W Erley *Surf. Sci.* **152 – 153** 142 (1985)
160. A Lock, J P Toennies, G Witte *J. Electron Spectrosc. Relat. Phenom.* **54 – 55** 309 (1990)
161. D L Adams, W T Moore, K A R Mitchell *Surf. Sci.* **149** 407 (1985)
162. K H Rieder, M Baumberger, W Stocker *Phys. Rev. Lett.* **55** 390 (1985)
163. G Witte, J P Toennies *Phys. Rev. B* **55** 1395 (1997)
164. M Yamaguchi, H Kaburaki, A J Freeman *Phys. Rev. B* **69** 045408 (2004)
165. G Armand, P Masri *Surf. Sci.* **130** 89 (1983)
166. A Kara, P Staikov, T S Rahman, J Radnik, R Biagi, H-J Ernst *Phys. Rev. B* **61** 5714 (2000)
167. M A Van Hove, G A Somorjai *Surf. Sci.* **92** 489 (1980)
168. K Jacobi, H Shi, M Gruytes, G Ertl *Phys. Rev. B* **49** 5733 (1994)
169. T Nagao, Y Iizuka, M Umeuchi, T Shimazaki, C Oshima *Phys. Rev. B* **55** 10064 (1997)
170. A P Graham, J P Toennies, G Benedek *Surf. Sci.* **556** L143 (2004)
171. P S J Bagus, P Batra, C W Bauschlicher, R Brae *J. Electron Spectrosc. Relat. Phenom.* **29** 225 (1983)
172. A Schmalz, S Aminpirooz, L Becker, J Haase, J Neugebauer, M Scheffler, D R Batchelor, D L Adams, E Bugh *Phys. Rev. Lett.* **67** 2163 (1991)
173. M Kerkar, D Fisher, D P Woodruff, R G Jones, R D Diehl, B Cowie *Phys. Rev. Lett.* **68** 3204 (1992)
174. M Kerkar, D Fisher, D P Woodruff, R G Jones, R D Diehl, B Cowie *Surf. Sci.* **278** 246 (1992)
175. C Stampfl, J Burchhardt, M Nielsen, D L Adams, M Scheffler, H Over, W Moritz *Surf. Sci.* **287 – 288** 572 (1993)
176. C Stampfl, M Scheffler, H Over, M Nielsen, J Burchhardt, D L Adams, W Moritz *Phys. Rev. Lett.* **69** 1532 (1992)
177. M M Nielsen, S V Christensen, D L Adams *Phys. Rev. B* **54** 17902 (1996)
178. Z C Ying, J Wang, E W Plumer *Surf. Sci.* **363** 289 (1996)
179. P Scharoch, J Neugenbauer, M Scheffler *Phys. Rev. B* **68** 035403 (2003)
180. R D Diehl, R Mc Grath *J. Phys.: Condens. Matter* **9** 951 (1997)
181. J Burchhardt, M M Nielsen, D L Adams, E Lundgren, J N Andersen *Phys. Rev. B* **50** 4718 (1994)
182. A Franchini, V Bortolani, G Santoro, V Celli, A G Eguiluz, J A Gaspar, M Gester, A Lock, J P Toennies *Phys. Rev. B* **47** 4691 (1993)

183. A Carlsson, A Hellsing, S-E Lindgren, L Walldén *Phys. Rev. B* **56** 1593 (1997)
184. S-Å Lindgren, C Svensson, L Walldgn *J. Electron Spectrosc. Relat. Phenom.* **64–65** 483 (1993)
185. N Fischer, S Schuppler, Th Fauster, W Steinmann *Surf. Sci.* **314** 89 (1994)
186. M Fuyuki, K Watanabe, Y Matsumoto *Phys. Rev. B* **74** 195412 (2006)
187. J H Petersen, C Søndergsrd, S V Hoffmann, D L Adams *Surf. Sci.* **461** 43 (2000)
188. D Tang, D McIlroy, X Shi, C Su, D Heskett *Surf. Sci. Lett.* **255** L497 (1991)
189. J M Carlsson, B Hellsing *Phys. Rev. B* **61** 13973 (2000)
190. H Ishida, Y Morikawa *Surf. Sci.* **291** 87 (1993)
191. G Witte, J P Toennies *Phys. Rev. B* **62** R7771 (2000)
192. A P Graham, J P Toennies *J. Phys. Chem. B* **105** 4003 (2001)
193. E Hulpke, J Lower, A Reichmuth *Phys. Rev. B* **53** 13901 (1996)
194. L Whitman, W Ho *J. Chem. Phys.* **83** 4808 (1985)
195. C Klünker, C Steimer, J B Hannon, H Ibach *Surf. Sci.* **420** 25 (1999)
196. J B Hannon, M Giesen, C Klünker, G Schulze-Icking-Konert, D Stapel, H Ibach, J E Müller *Phys. Rev. Lett.* **78** 1094 (1997)
197. K Watanabe, N Takagi, Y Matsumoto *Phys. Rev. B* **71** 085414 (2005)
198. C Astaldi, P Rudolf, S Modesti *Solid State Commun.* **75** 847 (1990)
199. P Rudolf, C Astaldi, S Modesti *Phys. Rev. B* **42** 1856 (1990)
200. S D Borisova, S V Eremeev, G G Rusina, S V Stepanyuk, P Bruno, E V Chulkov *Phys. Rev. B* **78** 075428 (2008)
201. V Eremeev, G G Rusina, E V Chulkov *Surf. Sci.* **601** 3640 (2007)
202. S V Eremeev, I Yu Sklyadneva, P M Echenique, S D Borisova, G Benedek, G G Rusina, E V Chulkov *Surf. Sci.* **601** 4553 (2007)

[a] — *Phys. Solid State (Engl. Transl.)*
[b] — *Russ. Phys. J. (Engl. Transl.)*
[c] — *Phys. Met. Metallogr. (Engl. Transl.)*